A 1.25 GIGABIT PER SECOND BINARY-PHASE-SHIFT-KEYED OPTICAL HOMODYNE RECEIVER

by

Igor D. Gonta

Submitted to the Department of Electrical Engineering and Computer Science in Partial Fulfillment of the Requirements for the Degrees of

BACHELOR OF SCIENCE

and

MASTER OF SCIENCE

at the

MASSACHUSETTS INSTITUTE OF TECHNOLOGY

June 1995

Signature redacted

Signature of Author. . . . . .
Department of Electrical Engineering and Computer Science
May 12, 1995

Signature redacted

Certified by. . . . . .
Dr. Jeff Livas, Member of the Technical Staff in the Optical Communications Group at the Massachusetts Institute of Technology Lincoln Laboratory
VI-A Thesis Supervisor

Signature redacted

Certified by. . . . . .
Jeffrey H. Shapiro, Professor and Associate Head of Electrical Engineering at the Massachusetts Institute of Technology
Thesis Advisor

Signature redacted

Accepted by. . . . . .
Frederic R. Morgenthaler, Chairman, Committee on Graduate Students

A 1.25 GIGABIT PER SECOND BINARY-PHASE-SHIFT-KEYED OPTICAL HOMODYNE RECEIVER

by

Igor D. Gonta

Submitted to the Department of Electrical Engineering and Computer Science
on May 26, 1995 in Partial Fulfillment of the Requirements for the Degrees of
Bachelor of Science and Master of Science

ABSTRACT

Optical communication receivers employing coherent (heterodyne or homodyne) detection, provide better sensitivity than do direct detection receivers. Optical homodyne receivers are 3dB more sensitive than optical heterodyne receivers, and are therefore attractive candidates for free space intersatellite communication links because laser powers on the transmitter end can be cut in half. In addition, homodyne receivers require less electronic bandwidth than their heterodyne counterparts because the optical signal is mixed down to baseband rather than to an electrical intermediate frequency. However, optical homodyne receivers require a phase-locked loop, in order to provide a phase reference for the detected data. This makes its design more complicated than the heterodyne case, for which frequency locking may be sufficient.

An optical homodyne receiver was constructed which employed synchronization bits to obtain a phase lock in the receiver. A transmitter was constructed that multiplexed in a synchronization bit every eighth bit into a 1.25 Gbit/s pseudorandom sequence. The phase-locked loop that was constructed was based on a decision-directed topology. However, because the phase noise information is encoded on the sync bit, the loop does not suffer any degradation due to data-to-phase crosstalk. Furthermore, because the sync bit does not completely modulate the optical signal, the loop retains the advantage of a residual carrier topology characteristic of a balanced phase-locked loop.

The overall system displayed the following performance. Phase locking was achieved with one laser acting as both the transmitter and receiver laser. The loop was observed to stay locked for as long as thirty minutes at a time. Frequency response measurements were made and were found to be consistent with the overall design of the phase-locked loop. A preliminary bit error probability measurement was made. The receiver was found to have a probability of error of 10^{-9} at 28 dB above the quantum limit of 9 photons per bit for binary phase-shift keying with homodyne detection. Significant improvements could be made to optimize the performance of the receiver both optically and electronically. In particular, reducing the electronic noise in the receiver is critical because it was this noise that dominated performance, not the local-oscillator shot noise of the homodyne detector.

Thesis Supervisor: Dr. Jeffrey H. Shapiro
Title: Professor and Associate Head of Electrical Engineering

Table of Contents

List of Figures

ACKNOWLEDGMENTS

Foremost, I would like to thank Dr. Jeff Livas for the technical knowledge and advice he has given me throughout my research. I thank Dan Castagnozzi wholeheartedly for the hours of electronics knowledge he gave me when I was debugging my circuit boards. I couldn't have done it with out you Dan. I would like to thank Dr. Roy Bondurant for his continued support and valuable insight. The support of everyone in Group 67 is also appreciated. Special thanks goes to the technicians in the group, especially Al Tidd, Josephine Capiello, Brian Lucia, and Diane Powers. I am grateful to Professor James Roberge for his valuable discussions on phase-locked loop theory. I would like to especially thank all of the members of Division 7 (Fabrication) at the MIT Lincoln Laboratory for their help in assembling and modifying my circuit boards. Special thanks goes to Gene Wessinger, and all of the technicians in the fabrication group, especially Tom who performed miracles on my boards. I acknowledge MIT Lincoln Laboratory for the generous resources made available to me.

On a more personal note, I would like to thank my parents foremost, for their continued support throughout my MIT education. I wish to thank my brother Alex for his useful engineering incite and the many interesting conversations we had about communications theory. My MIT and thesis experience would not have been the same without the numerous support of my fellow classmates and friends. I would like to thank all of my best friends for their overwhelming support and the faith they had in me to go on when I thought that I could not. I especially thank Nadia, Matt, Abbey, Jorey, Christine, Dan, Daisy, and Dianna. Deepest thanks goes to my roomate Alex for retrieving 99% of my thesis that I had lost due to a disk error. I would also like to thank all of my fellow brothers at the Alpha Epsilon Pi Fraternity for their continued support and the use of their laser printers. Thanks, the thesis looks great. Finally I would like to quote u2's Bono:

"I've conquered my past.
The future is here at last.
I stand here at the entrance of a new world I can see."

CHAPTER 1

INTRODUCTION

1.1 Background

With the quickly growing needs of the information age, the amounts of data that need to be transferred and the speeds at which they must be transferred are rising rapidly. This motivates the design and construction of high data-rate (several gigabits per second) communication systems. Free-space optical communication links, using optical heterodyne detection, are under development for providing high-rate intersatellite communications [3]. The energy-per-bit needed to achieve a particular error probability is fixed, for an idealized heterodyne receiver, so the total required optical power scales linearly with the data rate. At high data rates, this transmitter optical power can become hard to attain so it becomes necessary to seek receivers that are more sensitive than heterodyne detectors. Indeed, for typical intersatellite path lengths of about 40 thousand kilometers, the spreading of the laser beam power caused by diffraction dictates transmitter laser powers need to be of the order of one watt, for low error probability operation at data rates on the order of Gbps [3] Furthermore, the high power lasers must be diffraction limited. Currently, such high power laser technology is available. However, high power lasers can be expensive and inefficient. Optical homodyne detection may provide significant relief from this difficulty by reducing the transmitter laser power requirement.

1.2 Motivation

An optical homodyne receiver requires half as much signal power to achieve the same error probability as its heterodyne counterpart. A mathematical explanation of this fact will be provided in chapter 2. In addition, an intuitive understanding of this improvement can be gained from a frequency domain analysis of optical homodyne detection vs. optical heterodyne detection. This explanation will also be provided in chapter 2. It should be noted however, that a homodyne receiver provides a 3 dB improvement in sensitivity over a heterodyne receiver only in the optical case. In the electronic case, their sensitivities are equivalent [18].

For optimum receiver sensitivity, we not only require a homodyne receiver, but we also require an efficient modulation format. It is commonly known that Phase Shift Keying (PSK) provides the most improvement in sensitivity over other formats [11], [12], and [23]. Binary Phase Shift Keying (BPSK) is a fundamental version of this format in which the bit values zero and one are represented by transmitting alternate polarities (π radian phase shifting) of a single underlying waveform (i.e. a rectangular pulse). In general, one can build M-PSK receivers in which M>2 phase shifts are employed. Theoretically, a homodyne receiver is the most sensitive BPSK receiver one can construct. However, homodyne receivers are not without their disadvantages. They are more complicated to construct than heterodyne receivers because they require an optical phase-locked loop. In addition, they require narrow linewidth lasers to achieve good error probability performance [1], [6], [11], [14], [18]. These and other disadvantages will be discussed in chapter 3.

To illustrate the improvement in receiver sensitivity of an optical homodyne system vs. optical heterodyne systems (both BPSK and Binary Frequency Shift Keying (BFSK)), we can study Fig. 1 [2] on the next page.

Fig 1. is a plot of binary communication error probabilities vs. the number of received photons per bit for several different modulation/demodulation formats. The probability of error is one criterion that can be used in singular form to compare the

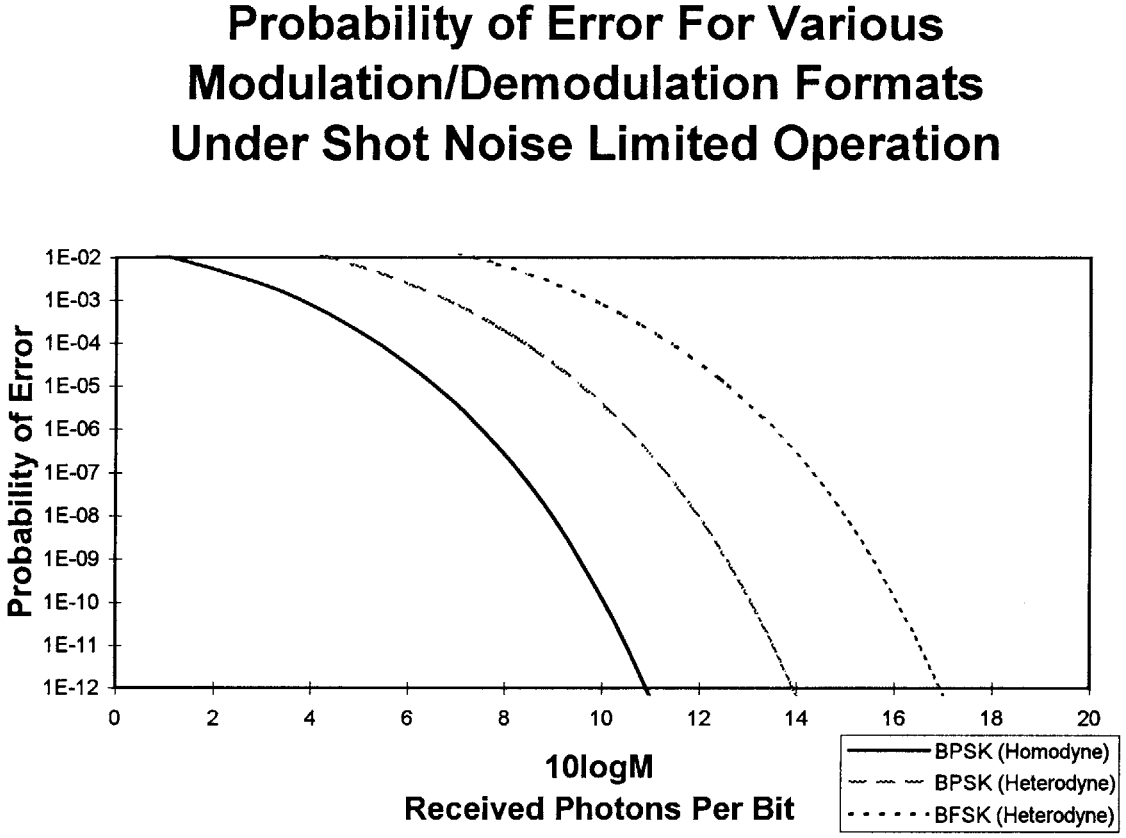

Fig. 1. Theoretical probability of error curves for three particular modulation/demodulation formats in the case of shot noise limited operation. As stated, BPSK optical homodyne is more sensitive than BPSK or BFSK optical heterodyne.

Where M is given by:

$$M = \frac{P_S \lambda}{hcR_b} \tag{1}$$

M = Photons Per Bit

P_S = Received Optical Power

λ = Wavelength of Transmitted Light

h = Planck's Constant

c = Speed of Light

R_b = Data Rate

capabilities of various receivers. From the plots, we see that BPSK homodyne receivers can achieve a desired bit error rate at a received optical power which is less than a BPSK heterodyne receiver. The curves also demonstrate that it is necessary to choose an efficient modulation format as well as a sensitive demodulation scheme, since BPSK heterodyne is better than BFSK heterodyne. The purpose of this thesis is to construct a 1.25 Gbit/s BPSK optical homodyne receiver.

1.3 Thesis Outline

Now that the goal for this thesis is clear, i.e., to build an optical homodyne receiver, the rest of this thesis is organized as follows: Chapter 2 will deal with the following: 1. An explanation of the BPSK modulation format, 2. a comparison of optical heterodyne to optical homodyne detection, 3. a qualitative analysis of several different topologies for phase-locked loops that can be realized in homodyne receivers, 4. a mathematical analysis of a decision directed loop and the implications of this analysis for certain design criteria for a receiver. Chapter 3 will include a proposal of the synchronization-bit receiver topology that was constructed. A comparison of this topology to the previously analyzed decision-directed loop will be made. Furthermore, an explanation of the receiver's operation will be provided. In addition to the discussion of the receiver design, an explanation of the transmitter design will also be provided because a transmitter had to be constructed to make the sync-bit topology receiver feasible. Chapter 4 will present the experimental results obtained, and will include discussion of these results. Finally, Chapter 5 will present some conclusions that were drawn from this work, and will look ahead into possible future improvements that can be made to the current design.

CHAPTER 2

THEORY

2.1 Binary Phase Shift Keying (BPSK)

In BPSK, binary digital data, i.e. a stream of "0's" and "1's", is encoded in the phase of the laser beam as a stream of 0 or π phase shifts respectively. Mathematically, the transmitted BPSK signal field (suppressing spatial and polarization characteristics) satisfies:

$$E_{sig}(t) = \sqrt{P_s}\cos(2\pi f_{opt}t + p(t)\pi + \Phi_s(t)) \tag{2}$$

$$p(t) = \sum_{k=-\infty}^{k=\infty} m_k\left[u(t-kT) - u(t-(k+1)T)\right] \tag{3}$$

Here, m_k. is the digital data stream, 1/T is the bit rate, and u(t) is the unit step function. P_s is the peak transmitted power of the laser which we assume to be constant. $\Phi_s(t)$ is the instantaneous phase noise of the signal laser. As we will see later, this phase noise will prove to be an important factor affecting BPSK performance. For the moment, we merely note that because BPSK encodes the data in the phase of the optical carrier, any phase noise adds to the uncertainty of the magnitude of the detected bit when a decision has to be made at the receiver.

Typically, we use an electrooptical device such as a waveguide phase modulator to impart the data onto the laser beam. At the receiver end of a coherent detection system, the optical transmitted signal is combined with a local oscillator laser beam in an optical coupler (a device that sums the electrical fields at its two inputs) and then photodetected. In a heterodyne system, the frequency of the local oscillator is different from the frequency of the transmitter laser. In a homodyne system, the frequency of the local oscillator laser is the same as the frequency of the transmitter laser, so the signal x local-oscillator beat

note in the photodiode's output is at baseband, i.e. in heterodyne terms the intermediate frequency of a homodyne receiver is 0 Hz. Thus, the detected signal contains only data and phase information and does not have a carrier frequency term. Mathematically, we have that:

$$E_{\substack{local \\ osc}} = \sqrt{P_{LO}}\cos(2\pi f_{opt}t + \Phi_{LO}(t)) \tag{4}$$

is the local oscillator field, and

$$i_{\text{det}}(t) = \alpha R(P_s + P_{LO} + 2\sqrt{P_{s,received}P_{LO}}\cos(p(t)\pi + \Phi_s(t) - \Phi_{LO}(t))) \tag{5}$$

is the output photocurrent from the detector. Here, R [A/W] is the detector responsivity. α is an amplitude factor which incorporates such factors as the coupling efficiency of light onto the photodetectors, polarization and spatial matching of the signal and local oscillator laser beams, etc. Also, (5) does not include any terms due to the noises in the receiver (such as shot noise) which would normally be present. We can see that the time-dependent term in (5) is independent of the carrier frequency since it is a homodyne system. The detected signal is the original waveform corrupted by the phase noise of the two lasers beating with each other at the receiver. Since this is the signal that will be operated on in the receiver to decide (in each bit interval) what bit value was sent, we can observe that it will be harder to make such a decision if there is a lot of phase noise present. In the case of a detected binary digital waveform, the degradation due to the phase noise will manifest itself as a partial closure of the detected data eye [12]. A more reliable decision can be made if this data eye is maximally open. Any closure of this eye due to noise will cause a degradation in receiver performance in the form of higher probabilities of error. We can understand the implications of equation (5) on receiver performance better if we interpret it graphically. Fig. 2 on the next page is a phasor domain representation of the transmitted signals. It also shows what the recovered data looks like.

BINARY PHASE SHIFT KEYING (BPSK)

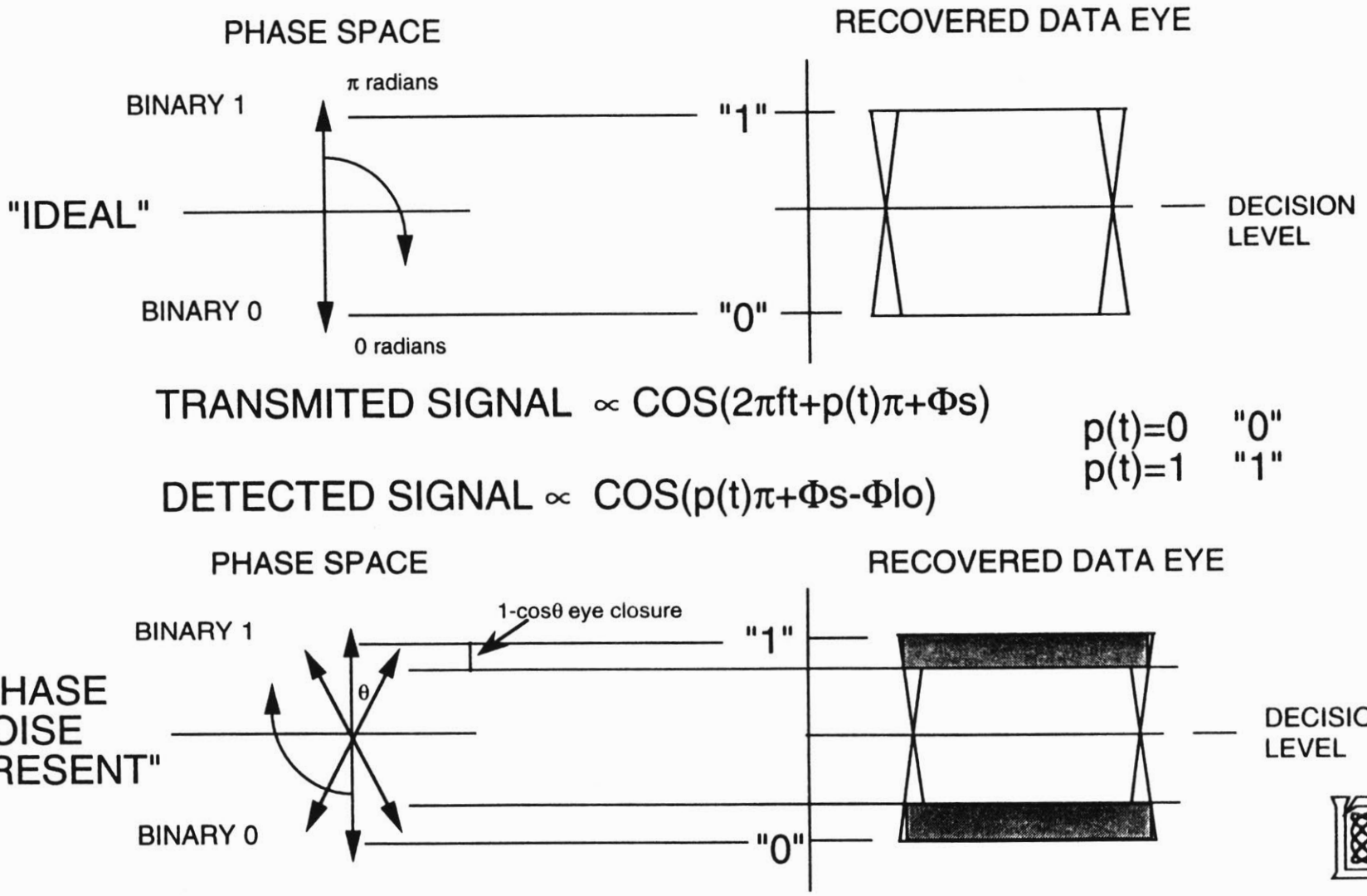

Fig. 2. Mathematical and graphical representation of Binary Phase Shift Keying (BPSK).

In phase space, we have a phasor rotating at the transmitted optical frequency. 0^0 and 180^0 phase correspond to a digital 0 and 1 respectively. At the receiver end, the detected signal maps to a voltage representation of the phase modulated data. In the top portion of Fig. 2, we analyze the ideal case in which there is no phase noise present in the detected signal. The only noise present is the local oscillator shot noise which is a quantum noise and cannot be eliminated. Thus, the best one can do is operate under a shot noise limited operation. For purposes of this figure, we only deal with the implications of the phase noise on the performance of the receiver. In the ideal case, the detected data "eye" is maximally open and a decision level can be chosen which will guarantee (provided there are no other sources of noise, i.e. electronic noise) a correct decision to be made on the bit detected. In this case, the receiver would operate at a 0 BER provided that the signal to shot noise ratio was high enough and that there was insignificant electronic noise. In the real world however, lasers have phase noise and this phase noise, many times characterized by a laser linewidth, may significantly affect the performance of an optical homodyne system. The effect of phase noise on the detected signal can be observed in the bottom portion of Fig. 2. Here, we have the phasor rotating at the optical frequency but in addition to this rotation, it jitters in time corresponding to the phase jitter imparted to the signal due to the noisy optical source. At the receiver end, this noisy signal is summed with a local oscillator which possesses its own linewidth, and the photocurrent from a square-law detector is proportional to this phase difference as shown in (5). When we translate this phase information into a voltage eye pattern, we see that the data eye closes by an amount proportional to one minuse the cosine of this phase noise (see figure). Thus, the signal-to-noise ratio is degraded and it will be harder to make a correct decision as to which bit was sent. Furthermore, under conditions of low signal-to-noise ratios, this noise can drastically affect the BER performance of the receiver. It is for this reason that we must be very careful in designing the receiver since we must suppress this phase noise as much as possible. The actual design criteria one must consider when designing a homodyne receiver will be dealt with in section 2.3.

2.2 Homodyne vs. Heterodyne Detection

To understand homodyne detection better, we can analyze Fig 3. given on the following page. First, we analyze the optical heterodyne case. Here, the transmitted optical signal is mixed with an optical local oscillator signal which is at a different frequency than the carrier and photodetected. The resultant signal is present at the difference frequency, or IF. In an ideal system, there is shot noise created at this photodetection stage and this noise sets the ultimate sensitivity limit for the receiver. Thus, the first Fourier transform representation shows the level of the signal and noise at the first detected stage. After the IF stage, the signal is further mixed down to baseband via an electronic multiplication by an electrical local oscillator operating at the IF frequency. Here, we can observe that the signal will add coherently but the noise will add incoherently. The noise is thus carried from the IF stage down to baseband and is twice as big as the base level of noise at the first mixing stage. The signal-to-noise is given by:

$$\left(\frac{S}{N}\right)_{HETERODYNE} = \frac{2TR^2 P_S P_{LO}}{qRP_{LO}} = 2M \tag{6}$$

Where M is as given in (1).

Now let us analyze the homodyne case. Here, the optical signal is detected directly down to the electronic baseband. The optical signal adds coherently. Since there is no IF stage, the only noise present at detection is the same level of noise that was present in the heterodyne case, since we are assuming an ideal shot noise limited receiver. Most of this noise is due to the local oscillator laser and we assume that the local oscillator laser power does not have any excess intensity noise. Thus, we save a factor of two in the level of noise present after the optical signal has been detected. Mathematically then, we have:

$$\left(\frac{S}{N}\right)_{HOMODYNE} = \frac{4TR^2 P_S P_{LO}}{qRP_{LO}} = 4M \tag{7}$$

HETERODYNE VS. HOMODYNE

HETERODYNE DETECTION

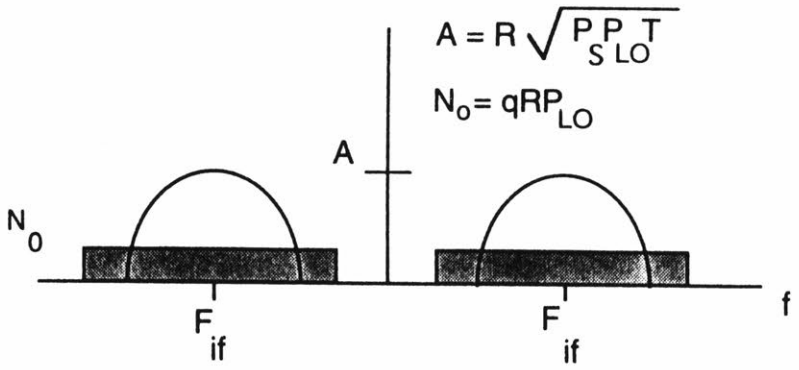

IF DETECTED STAGE

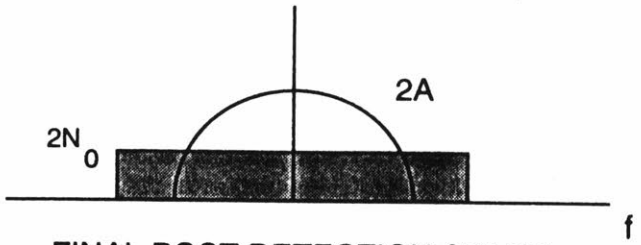

FINAL POST DETECTION STAGE
SIGNALS ADD COHERENTLY
NOISE LEVELS ADD INCOHERENTLY

$$S/N = \frac{4A^2}{2N_0} = 2M$$

HOMODYNE DETECTION

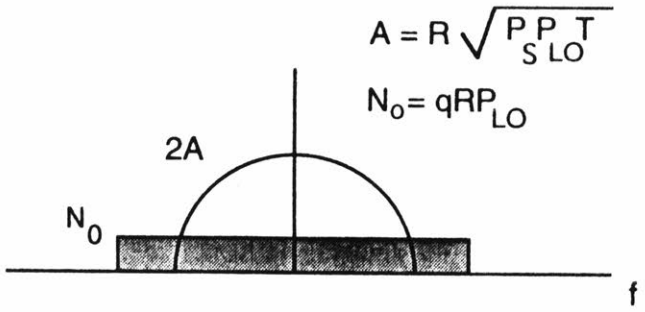

SIGNAL IS DETECTED RIGHT DOWN TO BASEBAND

BUT SAME LEVEL OF NOISE PRESENT AS
IN HETERODYNE RECEIVER

NOISE IN BOTH CASES IS DUE TO P_{LO}

$$S/N = \frac{4A^2}{N_0} = 4M$$

$S/N_{HOMO} = 2 * S/N_{HETERO}$ = 3dB IMPROVEMENT

Fig. 3. Comparison of heterodyne detection to homodyne detection.

Here we observe the theoretical 3 dB improvement in signal to noise ratios of optical homodyne receivers over heterodyne receivers for the same input power.

In addition to improved receiver sensitivity, a homodyne receiver provides other advantages over a heterodyne receiver. Homodyne receivers have higher bit-rate to detector bandwidth ratios. This is because transmitted information is detected directly at baseband, so the bandwidth of the receiver needs to be only on the order of the transmitted bit rate. This is not the case in a heterodyne receiver because information is centered around a nonzero IF. Thus, a heterodyne receiver needs a bandwidth approximately twice the data rate, which is centered on the IF. It is evident that this can become difficult to achieve electronically for very high data rates.

Although homodyne receivers are particularly attractive for high data rate communications for the above mentioned reasons, they are not without their faults. First, homodyne receivers require that the signal laser be frequency locked to the local oscillator laser otherwise an IF term will arise. Secondly, since no pilot carrier is transmitted, the phase reference for the signal is not present at the detector and an alternate one must be sought. This is particularly important with phase modulation transmission since all of the information is encoded in the phase of the signal. A phase reference must be established if reliable decisions will be made on the detected bits. One way to establish a phase reference is to make the phase of the local oscillator laser track the phase of the incoming signal laser (i.e., establish a phase lock in the system). If a phase lock is not established, then there will be no means of making reliable decisions on the received bits. One method of phase tracking in the receiver is to use a phase-locked loop to track not only the difference frequency between the local oscillator and the incoming signal but also the phase difference. To achieve a phase lock, an error signal must be produced in the receiver which is proportional to the phase difference between the signal and the local oscillator. This error signal is difficult to generate when there is modulation present and the phase information is encoded in the modulation. Thus, a phase-locked loop is typically difficult to construct for a BPSK signal. The complexity of the homodyne receiver design is one of its biggest disadvantages.

A necessary characteristic of any phase-locked loop is that they must somehow generate a voltage which is proportional to the error signal they are working to eliminate. As will be described in section 2.3, one way to obtain an error voltage that is linearly proportional to the phase difference between the signal laser and the local oscillator laser (i.e., the error that the phase-locked loop is trying to drive to 0) is to derive both an in-phase and a quadrature error signal from the received signal. An in phase signal is proportional to the received signal and a quadrature signal is the in-phase signal phase shifted by 90^{0}. These signals can be further processed electronically to produce the desired error signal in the phase-locked loop. An optical hybrid is one method used to generate such error signals which must be 90^{0} out of phase with each other. This hybrid is difficult to implement in fiber as will be discussed later.

Another disadvantage of a homodyne receiver is that it has very stringent laser linewidth requirements on both the transmitting laser and the local oscillator laser [6], [12], and [15]. This is because a homodyne receiver again lacks a carrier as a phase reference. Thus, the bigger the linewidth, then the more the data gets spectrally spread and the harder it is to obtain phase information. Even if a residual carrier were transmitted together with the encoded phase information, it is still a harder challenge to phase lock the signal to the local oscillator than to frequency lock them and this further adds to the complexity of the receiver design. So for the same BER, a homodyne receiver has to have less noisy lasers than its heterodyne counterpart. This amounts to building a very robust phase-locked loop which has good noise suppression and tracking ability.

2.3 Decision-Directed Phase-Locked Loop

Several different types of phase-locked loops can be constructed and each has advantages as well as disadvantages [5], [11], [12], [17], [24], and [25]. The most commonly used loops in optical receivers today include balanced, Costas, and decision directed loops. These loops were studied by the author of this thesis and a decision directed loop was chosen as a target for the design because it has the advantage of imposing a less stringent linewidth requirement than a balanced phase-locked loop or a Costas loop [11], [12], and [17].

To better understand a homodyne receiver, it is advisable to study a phase-locked loop in detail. By analyzing such a loop, we can identify the key parameters affecting overall receiver performance and we can focus the direction of a particular design topology. In particular, a decision-directed loop topology was chosen for the construction of the receiver for this thesis. Initial design goals were based on the theoretical calculations that will follow shortly. However, the final design deviated from the proposed design due to several factors such as availability of certain optical components. The design issues in the actual implementation will be discussed in detail in chapter 3.

Now we can analyze a decision directed loop. Fig . 4 on the next page shows a block diagram of a decision directed loop.

BLOCK DIAGRAM OF OPTICAL DECISION-DIRECTED PLL RECEIVER

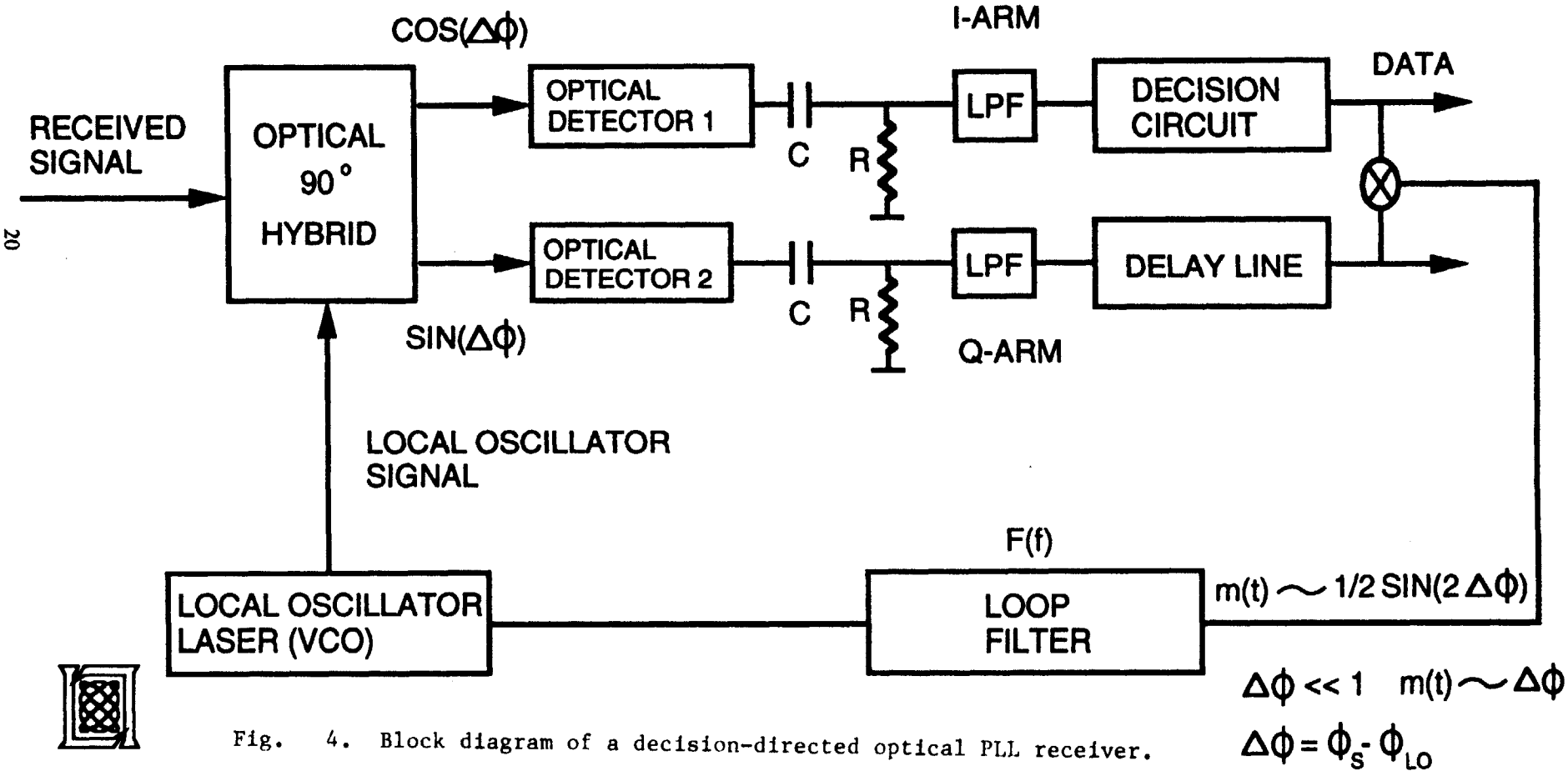

Fig. 4. Block diagram of a decision-directed optical PLL receiver.

The operation of the receiver is as follows. A received signal that is phase modulated enters the optical 90 degree hybrid. The signal contains phase information which corresponds to a binary representation of data. A binary "0" is encoded as a 0 radian phase shift and a binary "1" is encoded as a π phase shift for example. Here, this signal is optically mixed with a local oscillator laser signal that is at the same frequency as the transmitted signal. The interference terms in the output of the hybrid are independent of the carrier frequency. The two outputs of the hybrid are 90 degrees out of phase with each other. The top branch of the receiver is called the in-phase branch and the bottom branch is called the quadrature branch. These two signals are AC coupled to eliminate the DC components of the hybrid outputs. After low pass filtering to eliminate any unwanted noise present outside of the band of interest, the in-phase branch goes through a decision circuit and the detected signal is turned into digital data and sent to a BERT (bit error rate tester). The quadrature branch is delayed by the amount of time required for the decision circuit to operate on one bit and then is multiplied by the output of the in phase branch. This is done so that the signal produced is the sine of twice the phase difference between the signal laser beam and the local oscillator. This signal is independent of the data because the multiplication strips it off and thus data-to-phase crosstalk is eliminated (hence, decision-directed loop) if there are no detection errors. For small phase differences, the argument of the sine is small and it can be approximated through a Taylor expansion to be equal to just its argument. Thus, this multiplication produces a voltage which is linearly proportional to the phase difference. This signal is then fed back through a loop filter, which is basically an integrator, to try to drive this voltage down to 0. A 0 voltage means that the two lasers are phase locked. When a phase lock occurs, the BER decreases and valid data appears at the output of the receiver.

From the block diagram of the receiver in Fig. 4, several observations can be made. The first involves the realization that the lasers needed to be phase-locked must be frequency locked and that they must be relatively "quiet" otherwise the phase lock loop will not "capture" the signal. In addition, the linewidth of the lasers must be narrow since the spectral information is spread by the finite linewidth of the lasers and it becomes harder to track phase since a bigger bandwidth loop needs to be built to be able to track

out high frequency information. The second observation that can be made is that the overall loop delay of this receiver has an important bearing on the performance of the phase lock loop since it affects the amount of residual phase error present. Therefore, a loop of small delay will be desired. The remarks just made are only qualitative statements concerning receiver design issues. To obtain a better feel for the receiver design, it is necessary to quantify these statements. This necessity motivates a mathematical analysis of the decision directed phase lock loop.

Two important figures of merit in the design of the receiver are its error probability, Pr(e), and the residual standard deviation of phase error of the phase-locked loop, σ. The theoretical expression for the probability of error is given by Franz [6] as:

$$\Pr(e) = \int_{-\infty}^{\infty} \frac{1}{2} erfc(\sqrt{2M}\cos(\Phi)) \frac{1}{\sqrt{2\pi\sigma}} e^{\frac{-\Phi^2}{2\sigma^2}} d\Phi \tag{8}$$

where M is defined as in equation (1) and erfc is the complementary error function. The above equation is a result of a linearized loop analysis with Gaussian shot noise present. The expression only holds when the phase-locked loop is actually in lock. In addition, (8) assumes that the phase noise is varying slowly compared to the modulation rate.

In (8) we can see that the BER is a function of the received photons per bit which is directly related to the transmitted power. It is also a function of σ, the standard deviation of phase error due to noises present in the receiver such as phase noise and shot noise after the signal is processed by the phase-locked loop. Because of additive noise and phase dynamics, perfect phase estimation is impossible. It should be noted that (8) is a general equation for an optical homodyne receiver. Nowhere in the equation is the influence of a particular topology of a phase-locked loop present. Thus, we can only infer that to minimize the BER for a homodyne receiver, it is important to optimize the received power and the residual phase noise of some chosen loop.

The phase noise and shot noise for the decision directed loop of Fig. 4 with a Lorentzian-linewidth laser and a shot noise limited receiver have been analyzed by Norimatsu and Iwashita [15] and [16] and are given by the following:

$$\sigma^2_{TOT} = \sigma^2_{PN} + \sigma^2_{SN} \tag{9}$$

$$\sigma^2{}_{TOT} = \frac{\delta\upsilon}{2\pi}\int_{-\infty}^{\infty}\left|\frac{1-H(f)}{f}\right|^2 df + \frac{e}{4Rk_sP_s}\int_{-\infty}^{\infty}|H(f)|^2\, df \tag{10}$$

$$\sigma^2{}_{TOT}(k_s, P_s, \delta\upsilon, \tau_2, \omega_n, y) = \frac{\pi\tau_2\delta\upsilon}{2}F(y) + \frac{3e}{8Rk_sP_s\tau_2}G(y) \tag{11}$$

$$y = \frac{\tau}{\tau_2} \tag{12}$$

$$\tau_2 = \frac{\sqrt{2}}{\omega_n} \tag{13}$$

Here, the following parameters are given by:

P_S = Received Optical Signal Power

k_S = Fraction of Received Optical Power Devoted to Tracking. This ratio is determined by the optical hybrid.

$\delta\nu$ = Laser Linewidth

R = Photo Detector Responsivity

τ = Overall Loop Delay of Phase Lock Loop

ω_n = Loop Natural Frequency of Phase-Locked Loop

F(y), G(y) = Complicated polynomials in powers of y representing the integrals in (10)

H(f) = Overall Closed Loop Transfer Function of Second Order Loop

The above equations for standard deviation of phase error are particularly illuminating and it is worth discussing the receiver parameters on which they depend. We

observe that the standard deviation of phase error at the output of the phase lock loop is a sum of two components, one due to the phase noise of the lasers and one due to the shot noise of the photo detectors. In general, when the two components in this equation are exactly equal for a particular set of receiver parameters, then the standard deviation of phase error is minimum. This suggests that for a particular set of parameters, we have the ability to optimize our receiver such that it is operating at an optimum point. Minimizing this expression can lead to minimizing the BER for a particular desired signal to noise ratio. It is also worth mentioning that this expression only holds for the particular type of phase-locked loop that has been presented, namely a second order shot noise limited decision directed loop with lasers having a Lorentzian linewidth (i.e. white noise spectral density with no 1/f noise). Other loops of other orders would lead to different expressions. From Gardner [7], Blanchard [2], and other sources, we learn that a second order loop with a lead lag loop filter is an optimum choice for noise suppression. It also has other advantages over other loop topologies as well.

It is useful to plot the above expressions in order to be able to graphically interpret their meaning in the context of receiver design. Fig. 5 shown on the next page is a plot of the BER vs. S/N for different standard deviations of phase error in a phase lock loop.

BER vs. SIGNAL TO NOISE RATIO FOR A BPSK RECEIVER

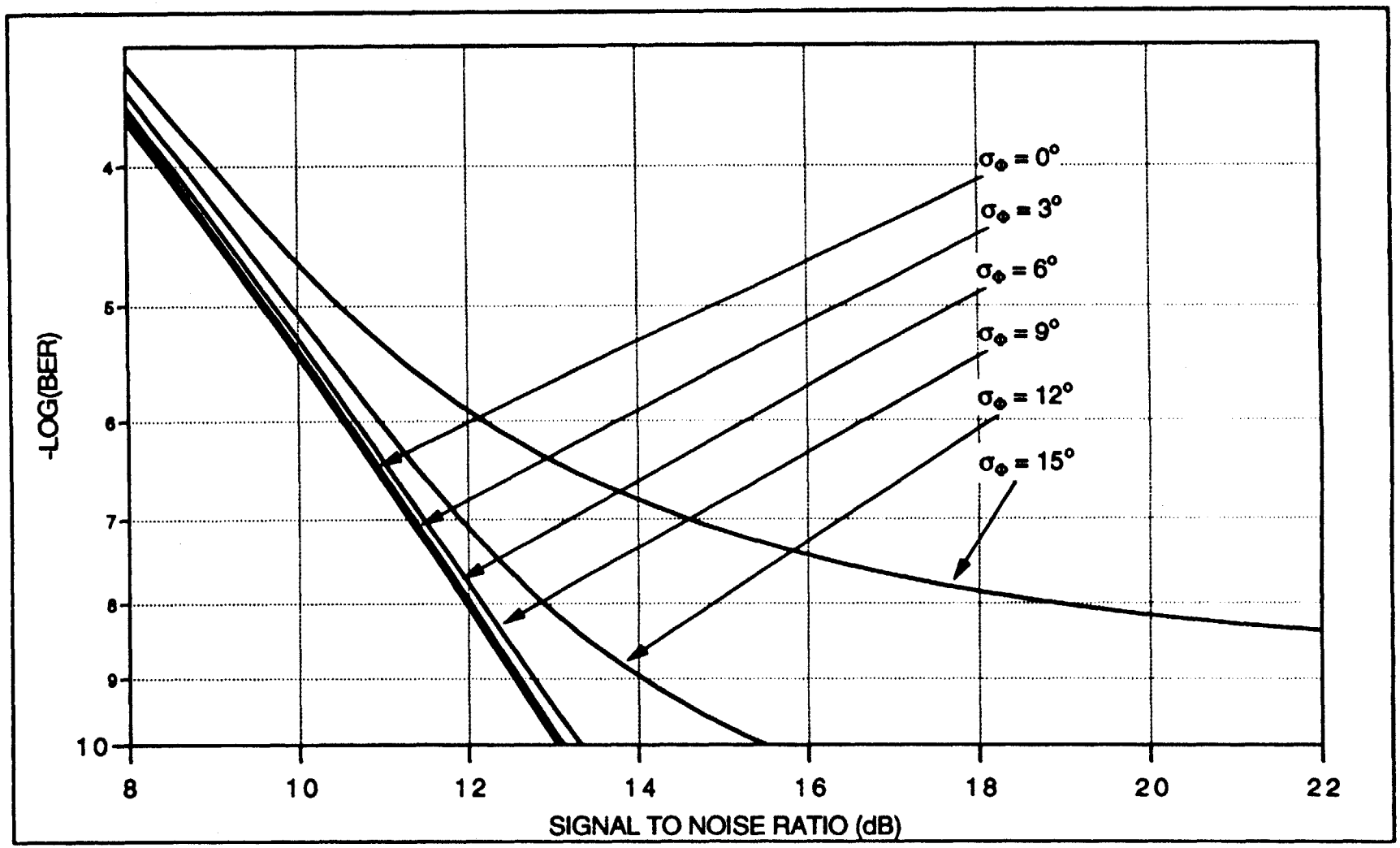

Fig. 5. Probability of Error vs. Signal-To-Noise Ratio for a BPSK Receiver.

It is quite evident from this graph that a reasonable target to choose for the standard deviation of phase error is approximately 9 degrees. This is because for any higher standard deviation, a considerably higher signal-to-noise ratio is required to achieve a probability of error of 10^{-9} which is the standard design spec for telecommunications. We must also note that the curves plotted here represent BER's for a PSK optical homodyne system. The particular loop one would use to achieve a residual phase standard deviation of error of 9 degrees has not been specified. To specify and determine the parameters of that loop, we must consider other constraints in the design of the system such as the linewidth of available lasers, finite loop delay due to the finite delay of available electronics, etc.

Another useful graph is shown in Fig. 6, which shows a plot of phase standard deviation of error vs. loop natural frequency for a second order critically damped decision-directed loop.

Phase Standard Deviation vs. Loop Natural Frequency For A Second Order Decision-Directed Phase-Lock Loop

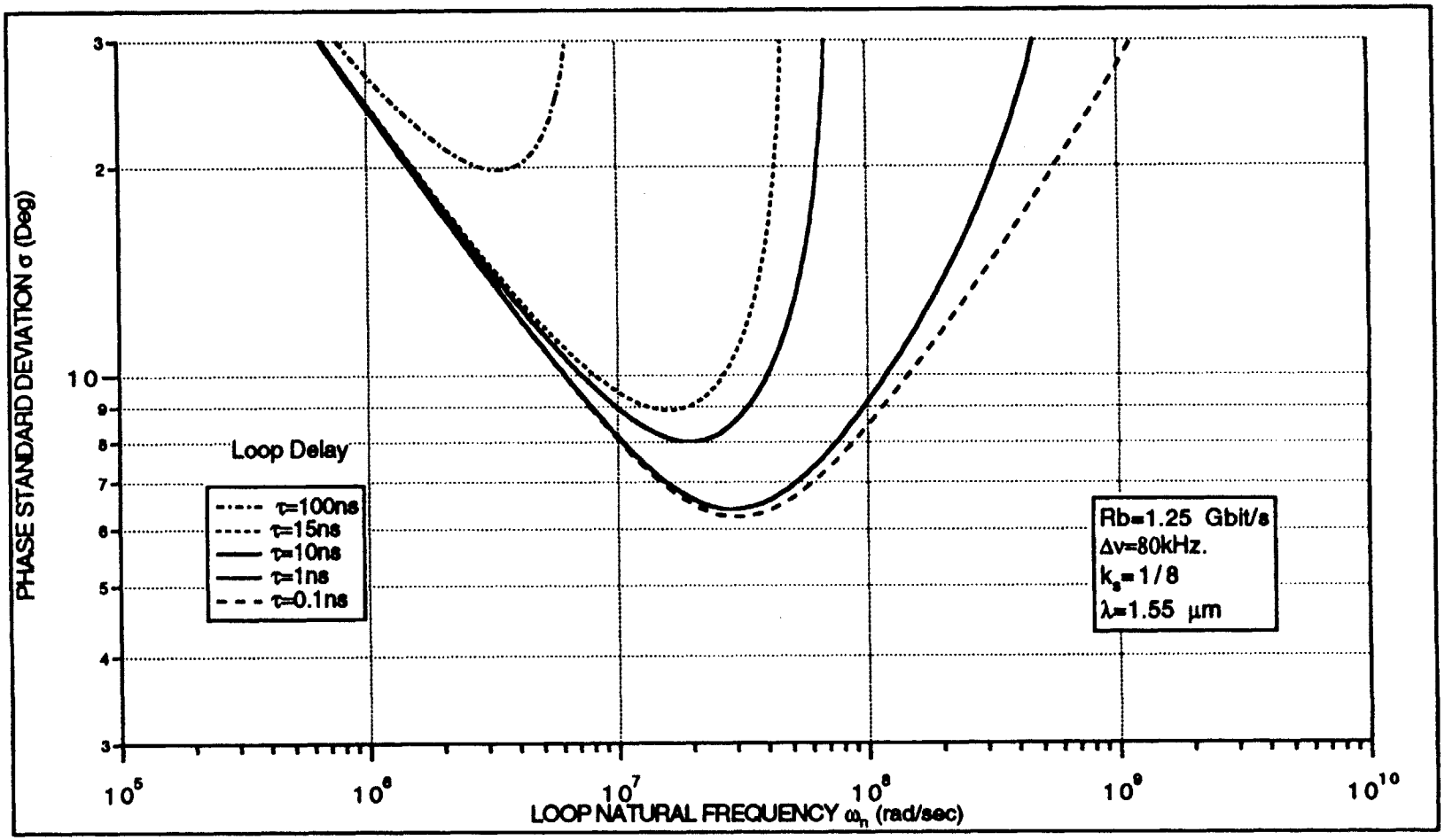

Fig. 6. Standard Deviation of Phase Error vs. Loop Natural Frequency for a Second Order Decision-Directed Phase-Locked Loop.

This is a particularly illuminating graph because of the obvious minima that arise. Given a particular loop delay, which is for all intents and purposes constrained by the design of the receiver, one obtains a curve that represents phase standard deviations for various loop natural frequencies. It is beneficial to choose where this curve has its minimum because that particular point will lead to a minimum residual standard deviation of phase error of the phase lock loop which will in turn help reduce the BER. So for example, given a 15 ns loop delay, one can observe which loop natural frequency will give a phase standard deviation of 9 degrees. If the 9 degree point does not occur at a minimum or worse yet if it does not even land on the curve at any point, then other parameters such as received power, laser line width, or power splitting ratio can be adjusted so the spec is met. It should also be noted that for the typical receiver parameters displayed in Fig. 6, one can deduce a reasonable splitting ratio to choose for the design of the receiver. It is found from other analyses, [11] and [12], not presented here that splitting ratios of more than 1/8 do not significantly reduce the phase standard deviation of phase error. Thus, it makes sense to pick $k_S = 1/8$ for typical receiver designs since there is no additional benefit to diverting any more of the received power than this from the communications portion of the receiver.

CHAPTER 3

RECEIVER DESIGN

3.1 Background and Introduction

Now that some generic phase-locked loop design issues have been discussed, it is necessary to discuss the particular receiver that was chosen for implementation in this thesis. It was found that an optical hybrid was very difficult to construct in fiber because the necessary optical components were unavailable. Specifically, polarization beam splitters could not be found which had the desired splitting ratios of approximately 90/10. This desired splitting ratio was deduced from the theoretical calculations that were performed on the decision-directed loop. It refers to the amount of received optical power one wishes to devote to communications and to phase tracking respectively. Since a decision-directed loop was still desired, another method was found which allowed for the construction of a homodyne receiver that did not require an optical hybrid. Wandernoth [26] has shown that a homodyne receiver can be constructed which uses synchronization bits to provide the necessary phase information for phase locking. Fig. 7 on the next page shows a block diagram of such a sync bit receiver.

SYNC-BIT RECEIVER BLOCK DIAGRAM

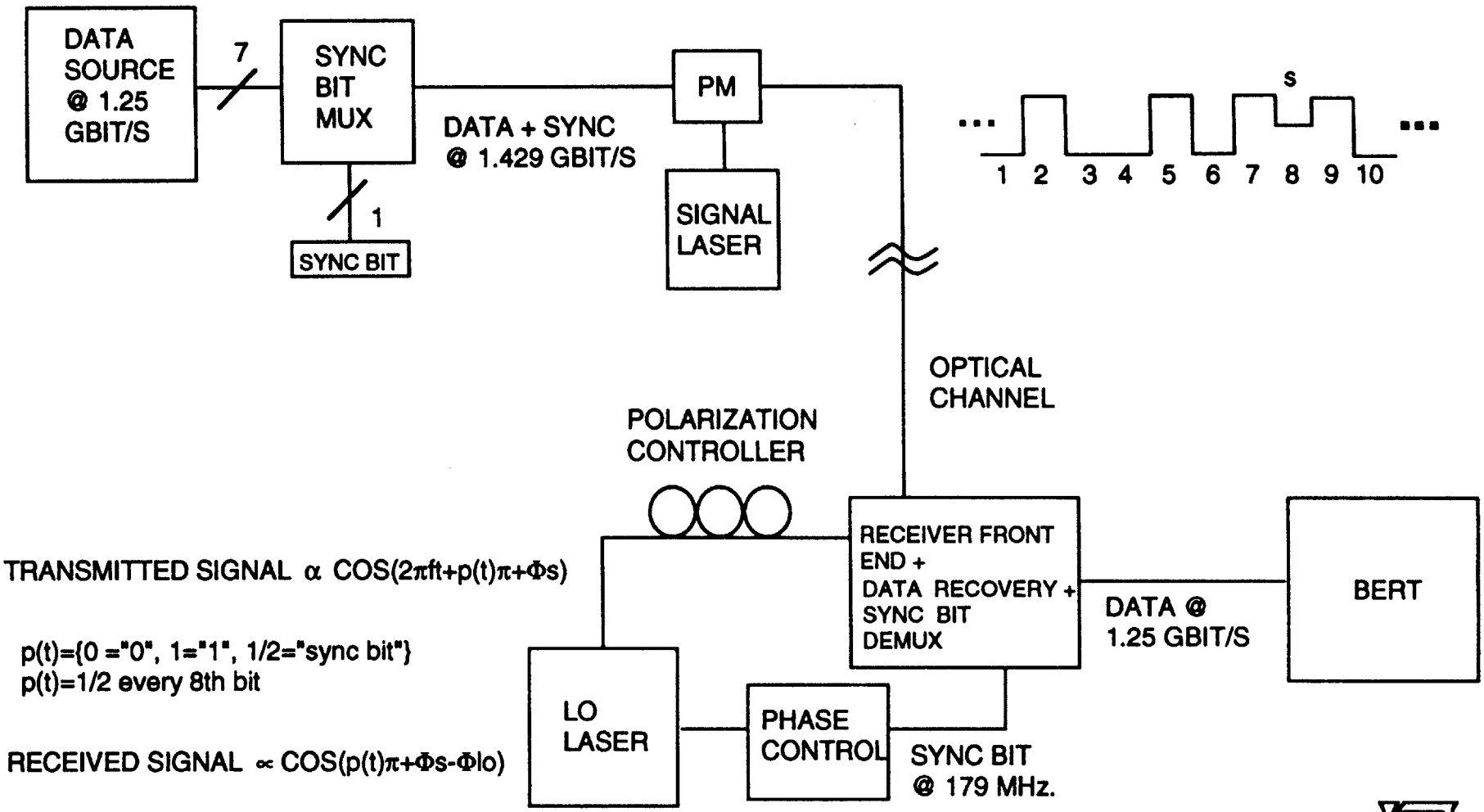

Fig. 7. Block diagram of the sync-bit receiver.

We can see from Fig. 7 that phase tracking is achieved by periodically sending a sync bit which is neither a "0" nor a "1" but is rather a half, along with the binary data. If the sync bit is sent every nth bit then it is the same as having a 1/n power splitting fraction between communication and phase tracking. Instead of devoting 1/n of the power in the signal beam to phase tracking, one is devoting 1/n of the time to phase tracking which amounts to 1/n of the power. At the receiver, we alternate in time between the "in-phase" and "quadrature arms". In order to send the sync bits, a transmitter must be constructed which will multiplex this sync bit stream into the real data. As stated before, a 1/8 splitting ratio is a reasonable design goal and so it was decided to make the sync bit every eighth bit sent. We can also see from the block diagram that the receiver must be able to demultiplex this sync bit, and use it appropriately in the feedback portion of the phase-locked loop. As will be explained later, an error voltage which is proportional to the phase difference between the signal laser and local oscillator can be generated from the sync bit. Thus, the need for an optical hybrid is eliminated and it is this feature which makes the sync bit topology attractive. However, the simplification of the optical portion of the receiver is realized at the expense of increased but realizable hardware complexity. In particular, a transmitter must be constructed which will multiplex in a sync bit every 8th bit into the data stream.

3.2 Sync-Bit Transmitter Operation

A schematic diagram of the transmitter is shown in Fig. 8 on the next page. The transmitter works as follows. Data at 1.25 Gbit/s is generated by a data source and is fed into the transmitter. In addition, a 1.25 GHz. clock is also applied. In this thesis, a 1.25 Gbit/s 2^7-1 pseudorandom sequence was used as the data stream. This data is clocked into a serial-to-parallel converter (1st. shift register) at 1.25 GHz. Seven parallel outputs are used and the eighth is terminated appropriately. The seven resulting lines go into a parallel-to-parallel converter that is clocked at 179 MHz. or 1/7 the rate of the original 1.25 GHz. clock. This slow clock is derived from the original clock by means of a 7 bit counter. A variable delay is used to phase the slow clock appropriately relative to the parallel data entering the parallel-to-parallel converter so that the setup and hold times are met for those signals. The function of the parallel-to-parallel converter is to up-sample the 1.25 Gbit/s data by 7. This allows for the original data to be separated into chunks of 7 bits so that later the 8th bit or sync bit can be multiplexed into the stream. The parallel data is fed into two 8 bit multiplexers simultaneously. The eighth line of one multiplexer is tied to a logical "high" and the eighth bit of the second multiplexer is tied to a logical "low". The final two multiplexers are clocked at 1.429 GHz (8/7 of the original 1.25 GHz. clock). This clock is derived by multiplying the 179 MHz. slow clock by eight using an active multiplier/phase-locked loop. The phase of this clock is also adjusted by means of a variable delay in order to meet the setup and hold times of the data signals relative to the two multiplexers. Finally, the output of the two multiplexers are added resistively to produce a tri-level digital signal. The data bits (high and low) add to their respective digital voltage levels and the eight low and high bits add to a voltage level midway between a logic low and a logic high. This final signal is amplified through a series of high speed amplifiers and is used to phase modulate the signal laser. In this way, the desired information is encoded in the phase of the transmitted light.

OPTICAL PSK SYNC-BIT TRANSMITTER

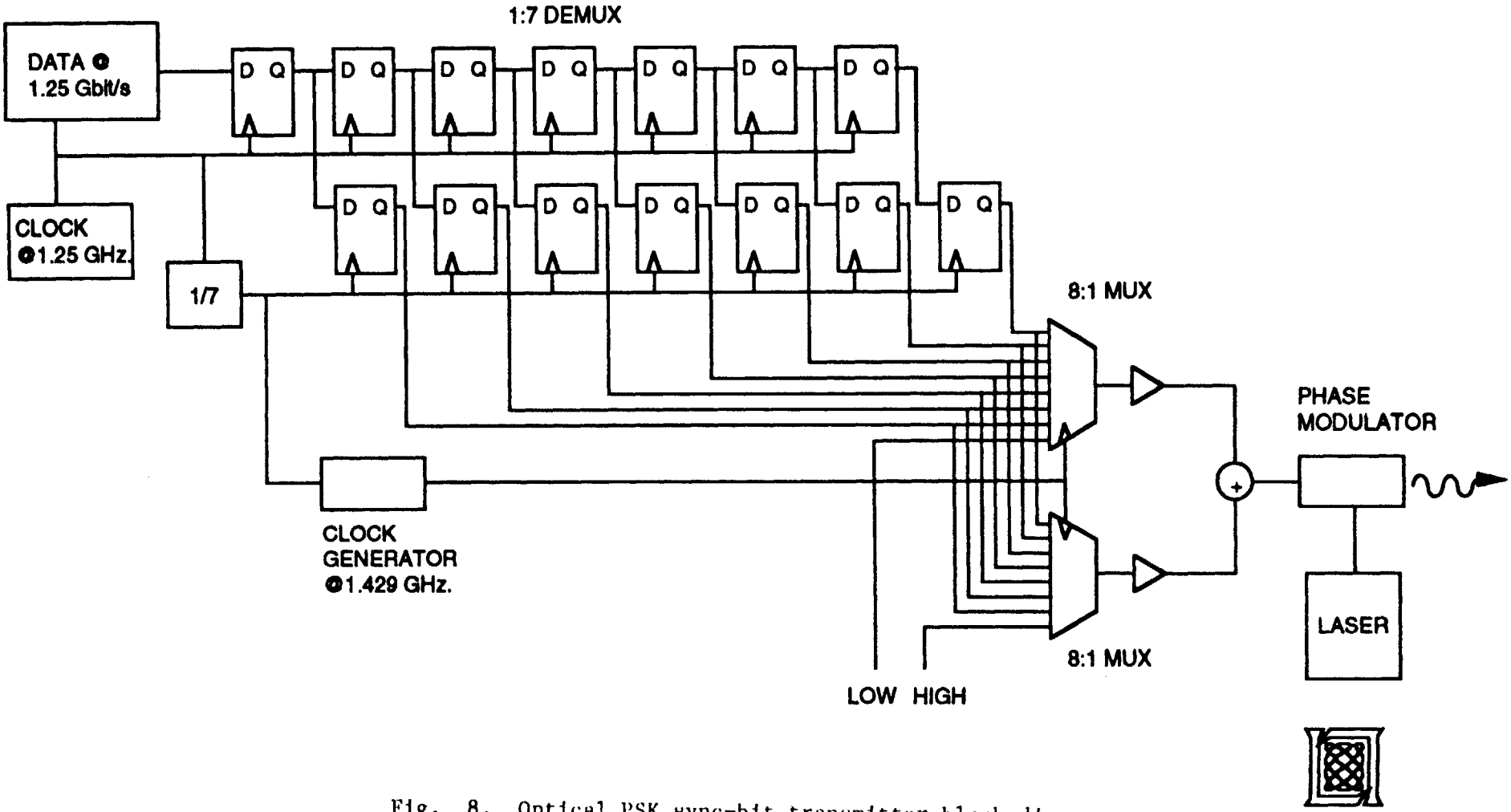

Fig. 8. Optical PSK sync-bit transmitter block diagram.

3.3 Sync-Bit Receiver Operation

Fig. 9 on the next page shows a schematic diagram of the optical receiver. The optical homodyne receiver works as follows: The transmitted light is mixed with the LO light in a 3-dB optical coupler and is detected by a pair of high speed photodiodes which are arranged in a balanced front-end configuration. A balanced front end is used in order to cancel the detected 0 frequency photocurrents that are produced by the photodetectors and to suppress local-oscillator excess noise. More importantly, the desired signal x local oscillator beat term is produced in this process; this term contains the transmitted data stream and the instantaneous phase information encoded on the sync bit. The resultant beat signal is amplified by a limiting amplifier. The limiting amplifier keeps the output signal amplitude constant for nonconstant input amplitudes. This is important because the detected signal will eventually be sent into a decision and clock recovery circuit. The clock recovery circuit provides a synchronized clock recovering the digital data. If a certain input level into the decision circuit is not maintained, then the circuit loses clock lock and the output data becomes unsynchronized. Thus, the limiting amplifier provides a constant amplitude signal which insures that the decision circuit doesn't lose clock lock.

After the signal is amplified, it is filtered. The filtering insures that any excess noise present outside of the band where data is present does not pass through and degrade receiver performance. The decision circuit proceeds to make a decision on every bit, including the synchronization bits. Thus, it produces a digital waveform at 1.429 Gbits/s (8/7 times the 1.25 Gbit/s data waveform) and a 1.429 GHz. recovered clock that is phase locked to this digital waveform. The resulting waveform is fed into an 8 to 1 demultiplexer which produces eight, 178.571 Mbit/s lines. Seven of these lines are data lines and the eighth line contains the sync bits. The seven parallel data lines are remultiplexed by a custom 7-1 multiplexer into a 1.25 Gbit/s serial data stream. This stream becomes the output of the receiver. The custom 7-1 multiplexer consists of a parallel-load serial shift-register that is clocked by a signal derived from the recovered clock of the decision circuit.

PSK OPTICAL SYNC-BIT HOMODYNE RECEIVER

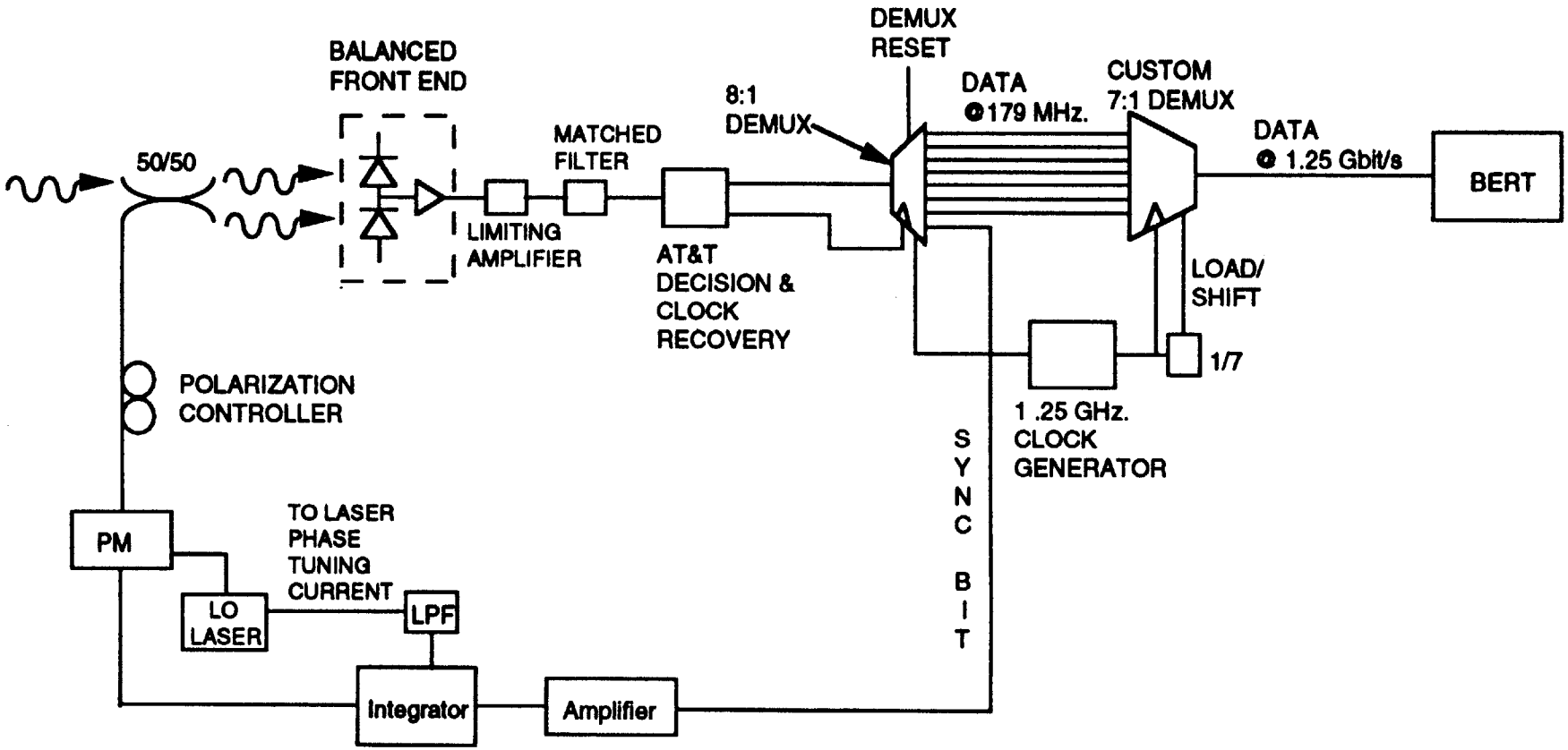

Fig. 9. PSK optical sync-bit homodyne receiver block diagram.

The sync bit is fed back and is used to derive the control signal for the phase-locked loop portion of the receiver. It must be noted that the sync bit must exit the appropriate line of the demultiplexer otherwise a data bit will be fed back and the loop will not acquire lock. To accomplish this task, a demultiplexer was chosen which could be electronically reset by applying a pulse from a push-button switch. Thus, to lock the loop, the switch had to be pressed until the sync bit came out of the appropriate line of the demultiplexer and was fed back in the phase-locked loop portion of the receiver.

A very subtle change occurs in the way the instantaneous phase difference between the signal and the local oscillator lasers is encoded in the sync bit. This change arises because the sync bit is operated on by the decision circuit. Since every sync bit becomes either a "1" or a "0", the phase information becomes encoded in the duty cycle of the resultant signal and thus it is the duty cycle of the new digital sync bit waveform which contains the instantaneous phase difference between the two lasers. In order to produce a signal whose amplitude is proportional to this phase difference, it is necessary to integrate the digital sync bit waveform. This integrated signal is applied to a phase modulator which controls the phase of the local oscillator signal. Since the phase variation of the phase modulator is a linear function of applied voltage, it, together with the integrator preceding it, acts as the VCO typically analyzed in the literature. Thus, the phase modulator completes the phase-locked loop portion of the optical receiver.

The sync bit design is, for the most part, consistent with the decision-directed receiver design that was analyzed in chapter 2. In the actual implementation, several factors were changed The first difference that can be noted is that two separate lasers were not used in the final setup. This was because two lasers were not found that had the narrow linewidth requirements and the desired frequency stability so that they could be mixed together and produce a true 0 Hz. IF. Two lasers could have been used if the initial design of the receiver had a provision for a frequency-locked loop in addition to its phase-locked loop. Thus, in the actual implementation, one laser beam was split in a 3 dB coupler, delayed by some length of fiber in both arms and then recombined to emulate two independent sources that were frequency locked. This set up will be analyzed later in this

thesis. In addition to this analysis, the particular laser that was used will be analyzed as well in terms of its impact on the performance of the phase lock loop.

The second difference arose in the way the actual loop was locked. Since the phase modulator or "actuator" in the control loop has only π worth of dynamic range, this put a limit on the dynamic tracking of the loop. Initially, the loop was observed to be locked for only a few seconds at a time, a period over which the phase difference of the two combined laser beams of light remained within π radians. This was because the phase of the lasers beating with each other in the 3 dB coupler was observed to undergo a slow variation of more than π radians. When the phase difference slipped by more than π, then the phase modulator reached its end of range, the loop would slip cycles, and the sync bit would slip as a result causing the loop to unlock. Thus, it was necessary to provide additional dynamic range in order to maintain loop lock for longer periods of time so that a bit error rate measurement could be made. To accomplish this task, several alternatives were considered. One way to stabilize the loop for a longer period of time involved matching the path lengths of the two arms in the optical setup better. This method would not insure a robust stabilization though because of environmental disturbances. Another way to increase the dynamic range of the loop was to choose a different actuator. One way to do this would be to use the error signal to control a PZT (piezo electric transducer). A PZT is a device which can alter the phase of a beam of laser light traveling through a fiber by applying a control voltage to the crystal around which the fiber is wrapped. The method that was chosen, however, was to feed back the error signal into the phase tuning current section of the laser that was used. To understand this arrangement better, it is necessary to understand the operation of the particular laser that was chosen.

The laser that was used in our setup was a DBR (Distributed Bragg Reflector) laser. This laser has two regions, one which lases when a bias current is applied above its lasing threshold and a phase tuning section located in the mirrors of the laser. A separate current can be applied to this phase tuning section which has gain in it. By applying current to this section, one can change the frequency of the laser. It was found that this current could adjust the phase of the detected signal waveform. The reason why a phase

change was imparted and not a frequency change was because only one laser was used. Thus, any frequency change was common mode to both beams combining at the 3 dB. coupler. However, because of a finite difference in path lengths that existed in both arms, the frequency change that was induced manifested itself as a phase change at the 3 dB. coupler. Thus, this additional control was used to provide more dynamic range in the loop since it was observed that this current provided controllable phase excursions over many π radians.

A DBR laser is a single-mode laser. However, since it can hop between many modes, it was necessary to pick a mode that had enough tunability over current to control the phase long enough to keep the loop locked for minutes at a time without slipping from one mode into another mode. In addition, the mode picked had to have enough gain or change of phase vs. applied current in order to have a robust lock. The approach that was taken to actually lock the loop was as follows. The error signal generated after the integrator was split and part of it was low-pass filtered by a simple one pole RC filter. This signal was applied to the phase tuning current section of the laser. The other half, or high frequency component, of the error signal was applied to the phase modulator. Thus, a nested phase-locked loop was achieved. The slow or low frequency component was used to track the slow, large dynamic-range random walk of phase difference between the signal and local oscillator beams. The fast control signal applied to the phase modulator was used to control high frequency phase variations of less than π radians between the two laser beams. Thus, the loop acquired more dynamic range to be able to track over many cycles of phase difference variation and could remain locked for a longer period of time.

In order to understand qualitatively how the actual phase-locked loop operates, it is necessary to understand the particular implementation more closely. One easy way to see how the loop acquires and maintains lock is to follow a frequency domain analysis of how the phase information is encoded in the sync bit and how it is used to track the phase of the signal laser. Essentially, the transmitter provides a 179 MHz. carrier on which the phase difference between the signal and the local oscillator lasers is sent to the receiver. In the time domain, this amounts to sampling of the instantaneous phase difference. The

detected signal is proportional to the sine of the phase difference between the signal and the local oscillator lasers. If this phase difference is small, then the sine can be approximated just by its argument and the resultant detected signal is a voltage which is just linearly proportional to the phase difference.. Under this approximation, the operation of the loop can be analyzed using simple Fourier transform techniques. Fig. 10 on the next page shows some key Fourier spectrum representations of phase signals at various points in the receiver and the transmitter.

TIME/FOURIER DOMAIN ANALYSIS OF SYNC-BIT RECEIVER

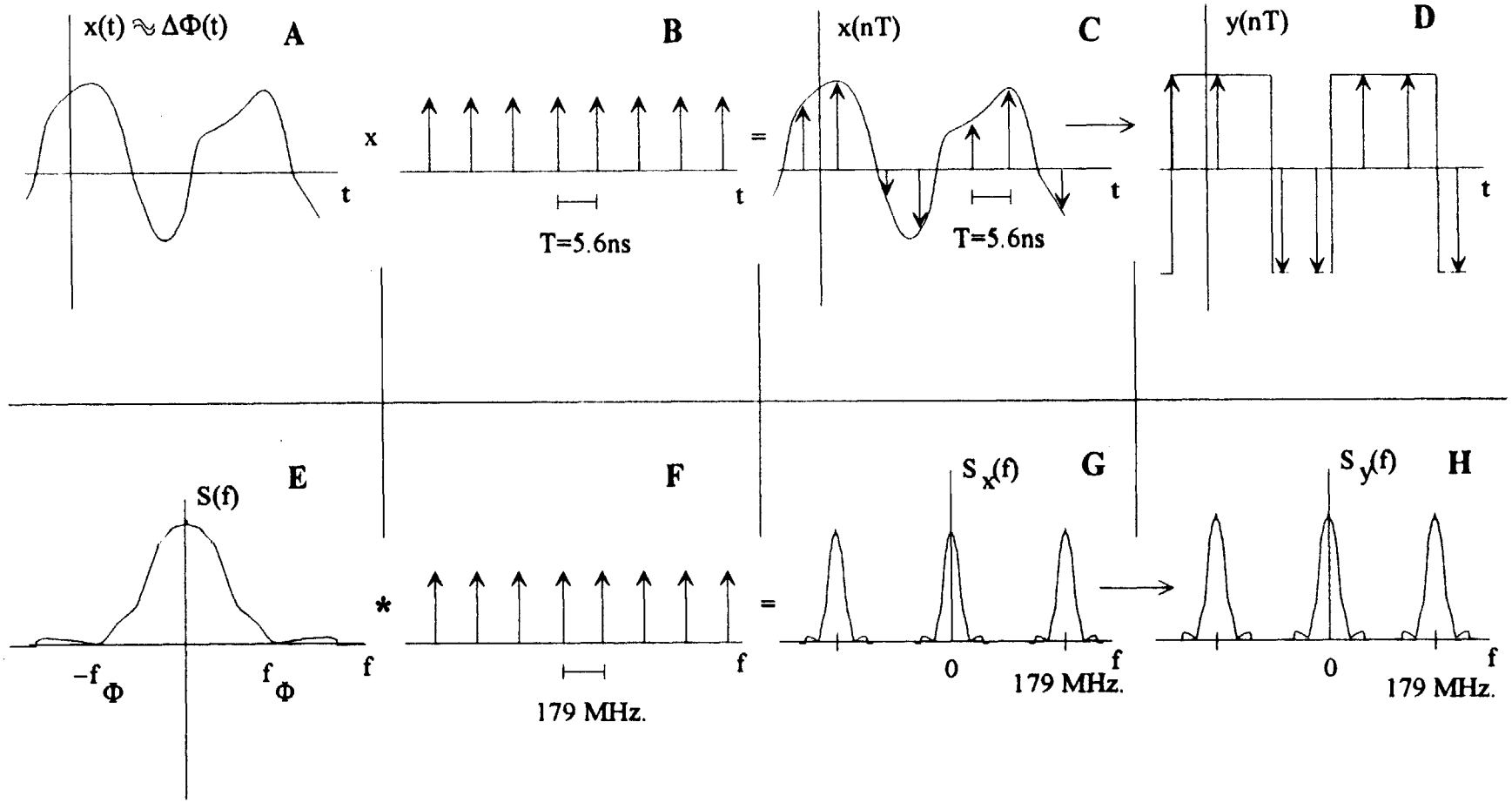

Fig. 10. Time/Fourier Domain analysis of sync-bit receiver operation.

Fig. 10 provides both qualitative time-domain representations as well as a frequency-domain analysis of the operation of the phase lock loop in the sync-bit receiver. This analysis only applies when the sync bit is considered in the context of the operation of the phase-locked loop (i.e. analysis of the operation of the quadrature-arm-equivalent of the decision-directed loop discussed earlier). In this figure, **A**, **B**, **C**, and **D** represent the time-domain analysis of the sync bit receiver. **E**, **F**, **G**, and **H** represent the corresponding frequency domain equivalents of this time domain analysis. Under the approximation of small differences in phase between the signal laser and the local oscillator laser, we can treat the detected sync bit signal as being linearly proportional to this phase difference. We can represent this phase difference as a stochastic process with some time function as done in **A**. **E** represents the power spectral density of **A**. The effect of the transmitter is to sample this time function at the sync bit rate as represented in **B**. In the frequency domain, this has the effect of copying the power spectral density of the phase noise at multiples of 179 MHz. (i.e. the sync bit frequency) as shown in **G**. Thus, it can be observed that one criterion for the sync bit topology to work is that most of the phase information be located in a frequency band which is less than half of the sample frequency (i.e. the Nyquist criteria) otherwise this information will be aliased and will degrade the loop's performance. In our system it was the case that we met the Nyquist criterion..

After the phase information is sampled, it passes through a decision circuit. The effect of the decision circuit is to take samples as represented in **C** and to convert them to constant amplitude samples as represented in **D**. Here, a change takes place in the way the phase information is encoded. It changes from being encoded in the DC level of the samples to being encoded in the duty cycle of the resultant waveform. Thus, the loop is locked when the duty cycle of the waveform out of the decision circuit is 50%. This duty-cycle modulation is converted back into an amplitude level by means of integration. This amplitude then provides the phase error correction that is imparted to the local oscillator laser by means of a phase modulator. In the frequency domain, the analysis of this stochastic process is more complicated. The exact analysis is provided in Papoulis [19]. There, the output power spectral density of the decision circuit is given and is related to the arcsine of the input power spectral density. In frequency, this amounts to a

convolution of **G** by the Fourier transform of this expression. The resultant spectrum is given in **H**. The exact expression is unimportant. What is important is the realization that the phase information has been encoded on the sync bit in the frequency domain in the form of a 179 MHz. carrier. It is this information which is low pass filtered (i.e. integrated) to provide the necessary phase control voltage to apply to the phase modulator. Another observation is that the phase information is independent of the data being transmitted since the phase information at the 179 MHz. carrier is in quadrature with the data at this same frequency. Thus, with the sync bit design, we do not experience data-to-phase crosstalk. To summarize, we can view the sync-bit transmitter/receiver pair as a means of encoding phase information at a specific carrier frequency and use this information to obtain a phase lock in the receiver.

CHAPTER 4

RESULTS

4.1 Experimental Procedure

After the optical receiver was constructed, it was necessary to test its operation. This process involved several steps. Here, we outline the method by which the receiver was characterized. In particular, we analyze the operation of the phase-locked loop and present the result of a measurement that was made to determine the parameters of the loop. Once we know these parameters, we can estimate the phase noise in the phase-locked loop and then proceed to calculate a theoretical probability of error curve for the receiver. Once this is accomplished, we can compare the theoretical prediction of the probability of error to the actual probability of error measurement that was made on the receiver.

4.2 Phase Lock Loop Parameter Measurements

We can model the phase lock loop in many equivalent ways depending upon which variables we wish to express as the ones that the loop is working to control (i.e. phase difference between the signal laser and the local oscillator, voltage, etc.). The approach that was taken was to model the loop using voltage as the state variable and then use this model to estimate the parameters of the loop. Once this was done, we could easily derive a new model where phase difference was the state variable without making any additional measurements. The reason why this approach was taken was because it was more feasible to make measurements on the loop which involved using voltage as the state variable. To understand how the measurements were made, we can analyze Fig. 11 on the next page which shows a block diagram of the optical homodyne receiver set up.

BLOCK DIAGRAM OF THESIS TABLE SETUP

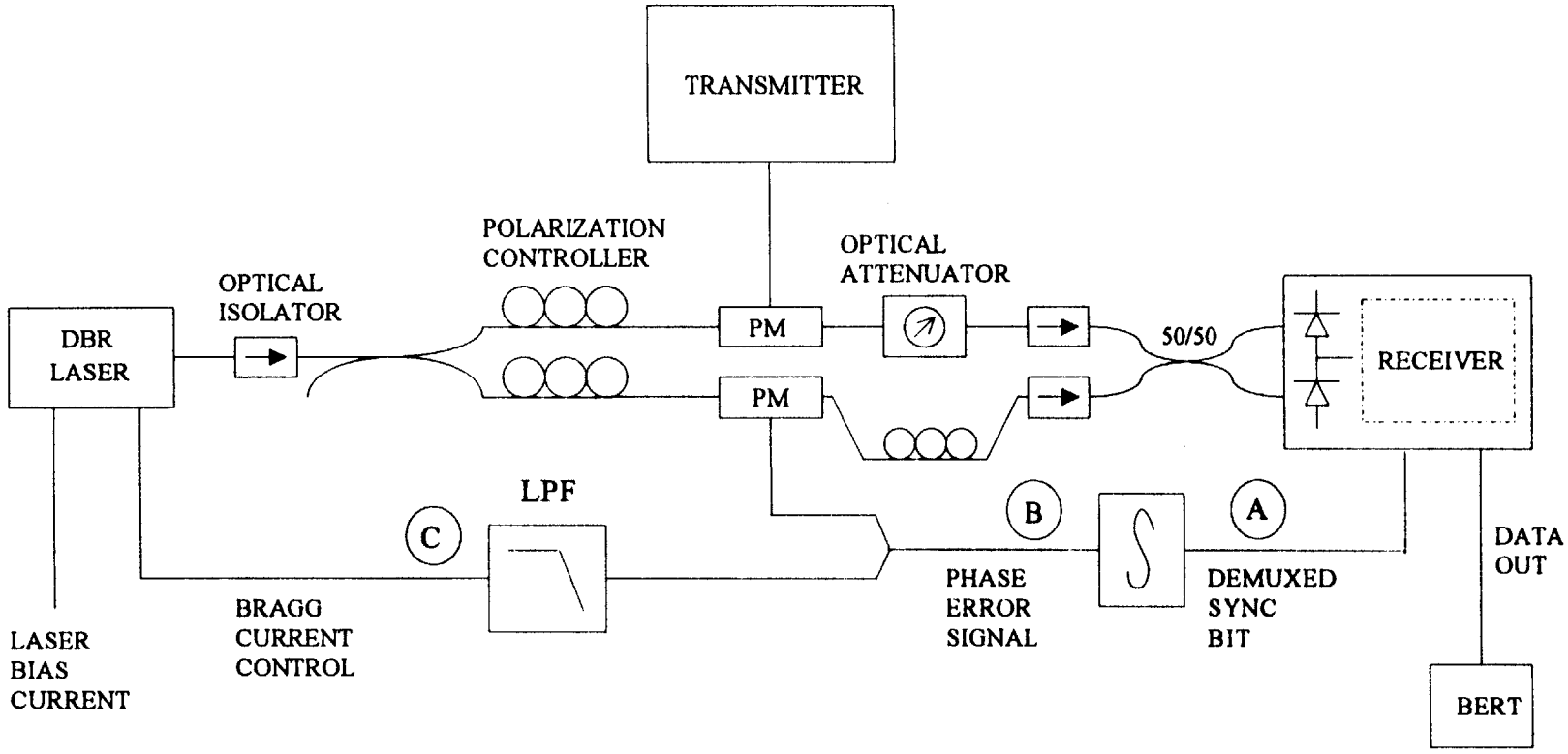

Fig. 11. Block diagram of thesis table setup.

Here, we see a block diagram of the setup that was constructed. It is easy to see the two loops that exist in the design in order to track out the phase noise in the loop and obtain a lock. For purposes of analysis, we must model these two loops in some fashion so that we can focus on the types of measurements we wish to perform. One way is proposed in Fig. 11. Points A, B, and C, represent three areas where the loop could be 'broken up" and thus abstracted into a block diagram. Points B to A represent one loop to analyze and points C to A represent another loop to analyze. To measure the response of the loop, it is necessary to do so under locked conditions. This is not a trivial task and care must be taken to understand exactly which parameters are being measured. The approach taken was to break the loop at point B (with C still locked) and inject a perturbation into the LO phase modulator. Then a signal could be measured after the integrator which would be the loops response to this perturbation. From this response, we could infer some loop parameters. This method is valid since the outer loop (i.e. C to A) maintains the loop in lock while the measurement is being made. Continuing with this proposal, we must now model the loop in such a fashion which corresponds to the description just given. Fig. 12 on the next page is a modeling of the measurements that were made.

PHASE-LOCKED LOOP BLOCK DIAGRAM

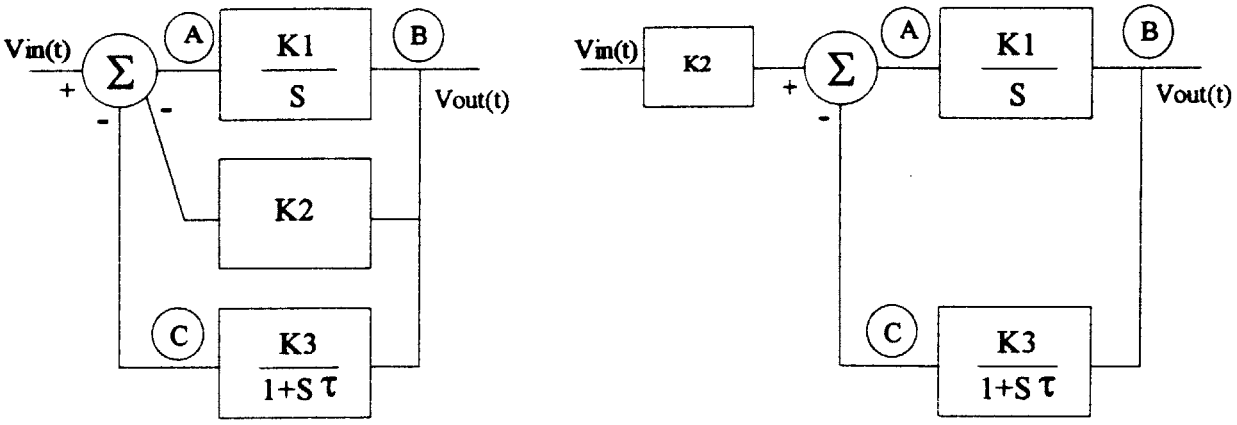

Block Diagram of Measurement Made

$$G(S) = \frac{K1*K2*(1+S\,\tau)}{S^2\tau + S + K1*K3}$$

$$G(f) = \frac{K1*K2*(1+j2\,\pi f\,\tau)}{j2\pi f - \tau(2\pi f)^2 + K1*K3}$$

$$K1 = 5100\ s.^{-1} = \frac{1}{2\pi(RC)_{int}}$$

$$K2 = .2$$

$$K3 = .6$$

$$\tau = 1.5 \times 10^{-3}\ s$$

Fig. 12. Phase-locked loop block diagram. Block diagram of measurements made is also shown.

The block diagram on the left represents the nested feedback paths just described. The task was to measure the unknowns, K1, K2, K3, and τ. If we treat the voltage at the summing node as the state variable, then we can compute a transfer function which models the behavior of the system under voltage perturbations. The block diagram on the right represents the measurement that was actually performed. The loop was broken at B and a signal from a dynamic signal analyzer was injected. The output was taken from point B and was fed into the second channel of the dynamic signal analyzer. A plot of the gain and phase of the transfer function could then be generated.

From the block diagram on the right, it is possible to compute the transfer function that was measured. Mathematically, we have:

$$G(s) = \frac{v_{out}(s)}{v_{in}(s)} = \frac{K1K2(1+s\tau)}{s^2\tau + s + K1K3} \tag{14}$$

The transfer function in terms of frequency is given by:

$$G(f) = \frac{K1K2(1+j2\pi f\tau)}{j2\pi f - \tau(2\pi f)^2 + K1K3} \tag{15}$$

From this equation, we notice the following facts:

$$G(0) = \frac{K2}{K3} \tag{16}$$

$$\lim_{f\to\infty}|G(f)| = \frac{K1K2}{2\pi f} \tag{17}$$

Thus, if we measure the transfer function correctly, under different limits, we may infer the parameters K2 and K3. The parameters K1 and τ were estimated and this estimation will be treated shortly. However, to infer K2 and K3, we must be confident that our

measurements are consistent with the predicted model of the transfer function. Thus, it was necessary to plot the magnitude and phase of the transfer function and compare it to the plot that was generated by the dynamic signal analyzer. First, we compute the magnitude and phase of the calculated transfer function:

$$|G(f)| = \frac{K1K2\sqrt{1+(2\pi f\tau)^2}}{\sqrt{(K1K3-\tau(2\pi f)^2)^2+(2\pi f)^2}} \tag{18}$$

$$\angle G(f) = \tan^{-1}(2\pi f\tau) - \tan^{-1}\left[\frac{2\pi f}{K1K3-(2\pi f)^2\tau}\right] \tag{19}$$

If we plot the magnitude and the phase, we can compare it to the actual measurement taken. Figs. 13 and 14 on the next page present this comparison.

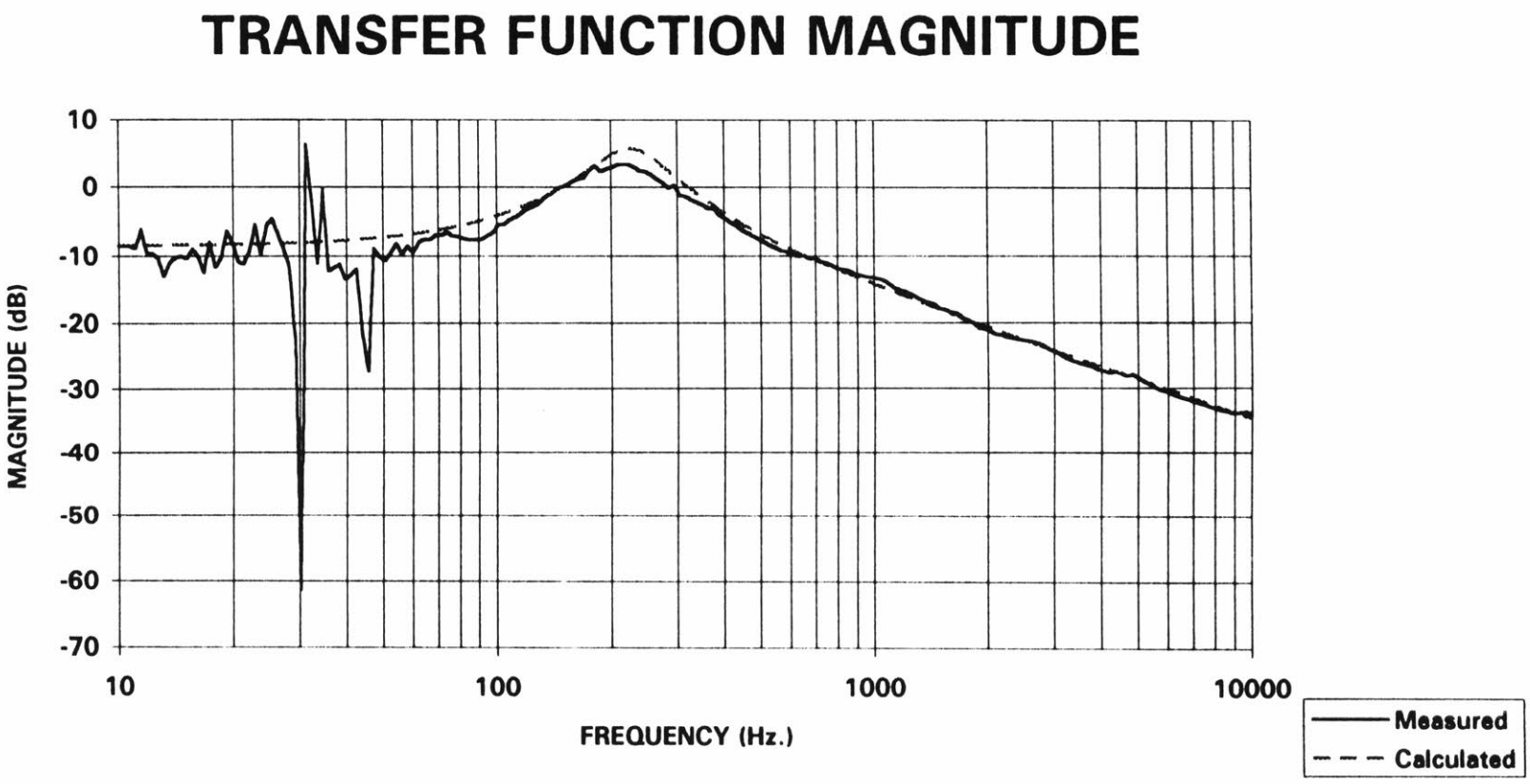

Fig. 13. Magnitude of transfer function. Measured and calculated curves are shown.

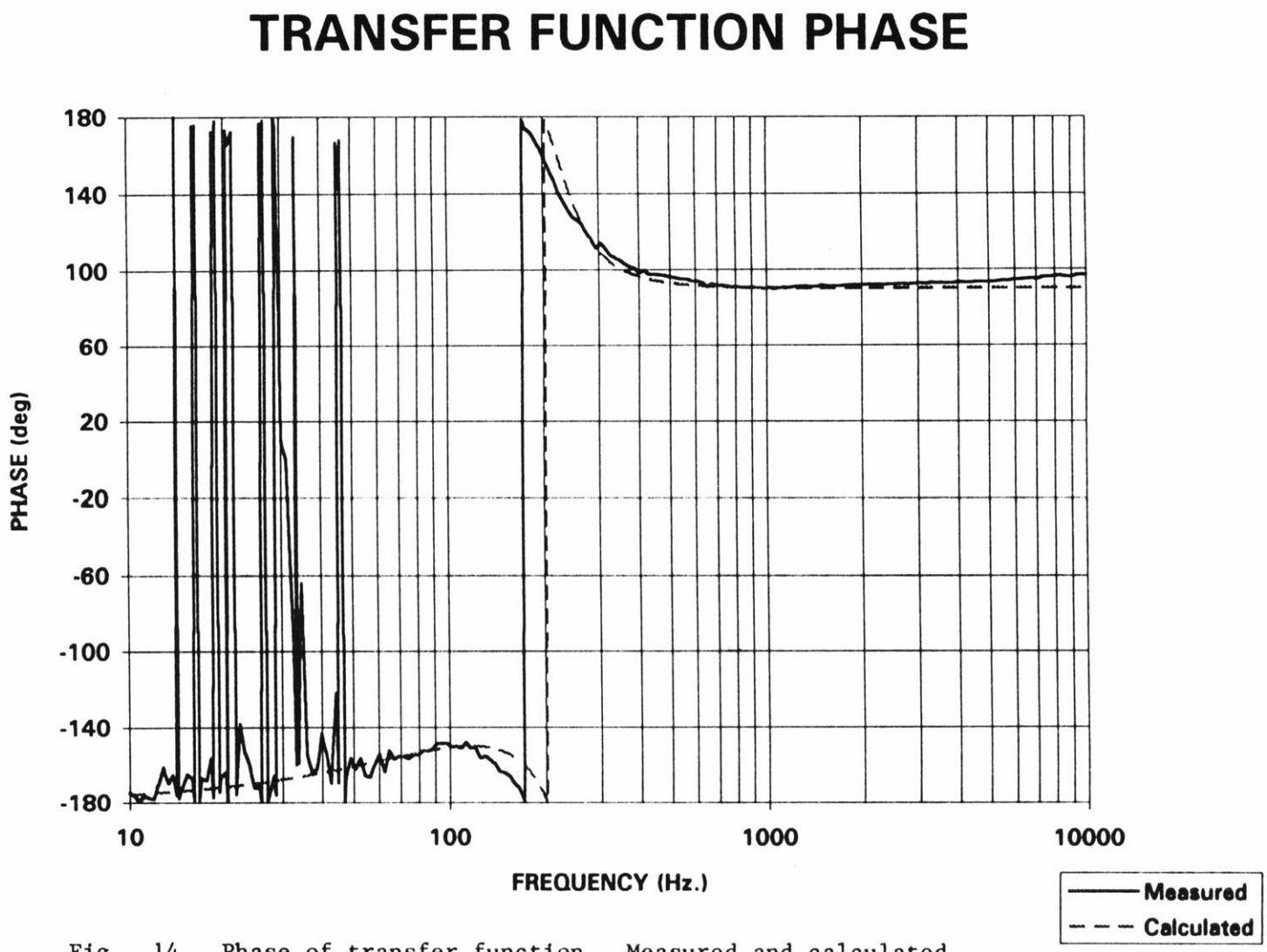

Fig. 14. Phase of transfer function. Measured and calculated curves are shown.

The measured and calculated plots agree with each other fairly well. Places which show a slight discrepancy between the measured data and the calculated gain and phase are probably due to a certain degree of error that was made when estimating the parameters K2 and K3 from the measured data. This estimation was done according to (16) and (17). Values were obtained from the actual measurement under the different limits and the correspondingly, K2 and K3 were calculated based on those values. In addition, the value of K1 was calculated according to the time constant value that was built into the integrator and τ was also calculated according to the values chosen for the time constant built into the low-pass filter. These values as well might contain some errors in them. The point in the measurement of the magnitude of the transfer function which is spiky is due to the fact that the loop went out of lock during that time. Thus, those data points are not reliable and were not used to estimate any of the desired parameters. The glitches in the plot of the measured phase of the transfer function may be due to the fact that the loop went through many π radians of phase shift but did not go out of lock during that time.

Since we are fairly comfortable with the agreement in Figs. 13 and 14, we can be confident in the values obtained for K1, K2, K3, and τ. These values are given by:

$$K1 = \frac{1}{2\pi(RC)_{\text{int egrator}}} = 5100 s^{-1}$$

$$K2 = .2$$

$$K3 = .6$$

$$\tau = 1.5 \times 10^{-3} s$$

Here, K2 and K3 were derived from the measurement as explained. K1 is the integration time constant of the integrator in the loop and was calculated from the RC value used. τ was chosen to make the cutoff frequency of the low pass filter approximately 100 Hz. The particular choice of these two values was to a first approximation, fairly arbitrary. The goal was to lock the loop first, with reasonable values of loop parameters, and then to attempt to make a measurement of the receiver loop transfer function. Once this could be

accomplished, then a better understanding of the loop could be attained and further optimizations could theoretically be implemented to the loop parameters. The impact of the parameters that were initially chosen on the performance of the receiver will be discussed later.

4.3 Phase Lock Loop Noise Analysis

Now that these values for the loop were obtained, it was necessary to remodel the loop using phase as the variable. Doing so would allow for the proper analysis of noise in the loop. Once a better understanding of the noise could be attained, calculation of the standard deviation of phase error in the phase lock loop could be achieved. Knowing this quantity, we could proceed to calculate a theoretical probability of error curve for the receiver. This curve could then be compared to the actual probability of error curve that was measured. Thus, it was necessary to redraw the loop in terms of voltage to phase and phase to voltage gains. Such a model is shown in Fig. 15 on the next page.

PHASE-LOCKED LOOP BLOCK DIAGRAM

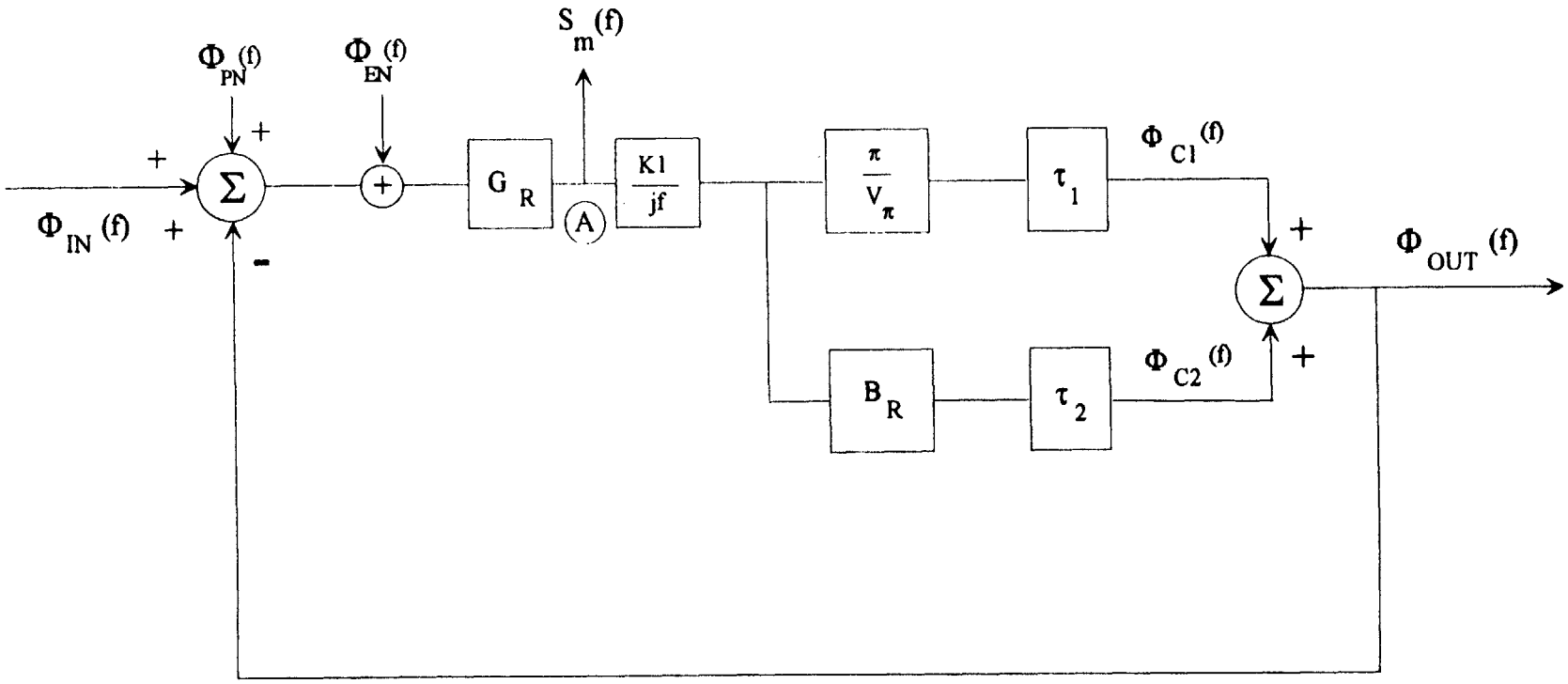

Fig. 15. Block diagram of phase-locked loop showing phase as the key variable of interest.

In Fig. 15, we have shown the phase-locked loop portion of the sync bit receiver. Here it is obvious that the action of the loop is to use feedback to control the phase difference between the signal laser and the local oscillator laser. In general, this phase difference will have some power spectral density and can be treated as a phase noise being summed in at the input to the receiver. This can be observed at the first summing node. A shot noise term would also be present at the summing node but after measurements of the shot noise were made and were compared to the electronic noise measurements of the receiver, we observed that the electronic noise dominated. It is this noise that is shown to be added at the first summing node in the block diagram of Fig. 15 and not the shot noise. Thus, the receiver is not shot noise limited and this term is insignificant to the overall noise that the phase lock loop must work to suppress.

In addition to the power spectral density of the phase noise, the other significant noise term, as was already mentioned, is the electronic noise of the receiver due to amplifier thermal noise, etc. This noise in general will also have some power spectral density and can also be treated as additive noise in the receiver. Thus, it is these two noises that the phase lock loop is trying to suppress in order to obtain a phase lock. Now that the loop is modeled in an appropriate fashion, we may proceed to calculate the phase noise spectrum that we expect to see in the receiver. For measurement simplicity, we chose to measure the power spectral densities at point **A** in Fig. 14. Here, the measurements that were made were a voltage spectrum denoted by S_m (f) in [Volts^2/Hz]. To convert these quantities to phase noise spectral densities [Rad^2/Hz.], we would divide by G_R^2, the square of the effective phase-to-voltage gain of the receiver as represented in Fig. 15. Thus, we could take measured electrical quantities and by the appropriate normalization, scale them back to the input summing node in Fig. 14 in terms of their phase-noise equivalents.

Several noise power spectral density measurements were taken. These included measurements of the phase-locked loop unlocked, locked, electronic phase noise, shot noise, and the noise of the measuring device including the measuring probe. We found that the receiver was dominated by electronic phase noise, because the shot noise in comparison with this quantity was insignificant and there was no difference in the noise

level with the LO laser light on or off.. The reason why the electronic noise dominated is because there was not enough local oscillator optical power to overcome the thermal noise of a 50Ω load. Additional noise might also have been present due to noisy amplifiers in the circuit. Thus, we could not expect the receiver to be dominated by shot noise. All measurements were done at point **A**. To make the unlocked measurement, both loops were broken at point **A** and the spectrum was taken. Then the receiver was brought under lock and the measurement was taken again under closed loop conditions. Finally, it was necessary to predict the action of the phase-locked loop. To do so, we attempted to theoretically predict the closed loop phase noise spectrum of the receiver. Mathematically, we must have the following hold:

$$S_{\Phi,locked}(f) = |A(f)|^2 S_{\Phi,unlocked}(f) \tag{20}$$

Where we have,

$$S_{\Phi,unlocked}(f) = \frac{1}{G_R{}^2}(S_{PN}(f) + S_{EN}(f)) \tag{21}$$

And A(f) is the appropriate transfer function for the measurement that was made. A(f) is given by:

$$A(f) = \frac{G_R}{1 + \frac{G_R K1}{j2\pi f}\left(\frac{\pi}{V_\pi}e^{j2\pi f\tau_1} + B_R e^{j2\pi f\tau_2}\right)} \tag{22}$$

$$G_R = K2'\frac{V_\pi}{\pi} \tag{23}$$

$$B_R = \frac{K3}{G_R(1 + j2\pi f\tau)} \tag{24}$$

$$K2' = K2\frac{\sqrt{i_S i_{LO}}}{\sqrt{i_{S,Measured}, i_{LO,Measured}}} = 1.1K2 \tag{25}$$

$$V_\pi = 8V \tag{26}$$

In (22), τ_1 and τ_2 represent the loop delays in the two loops of the phase-locked loop. Measurements of these quantities were made and they were found to be 60 ns and 162 ns respectively. These quantities would significantly affect loop performance if our loop had been a high bandwidth loop (i.e., MHz. bandwidth). However, the loop that was actually built was a low-bandwidth loop, operating in the regime of several hundreds of hertz. Thus, the exponentials in the above equation can be treated as unity to a first approximation without much loss of accuracy in the calculation of the transfer function A(f). It should also be worth mentioning the following observations: First, we must realize that G_R (the "effective phase to voltage gain" of the receiver model) is in general, a function of frequency rather than a constant. The cutoff frequency of G_R is approximately 1 GHz. which is the cutoff frequency of the electronic filter in the receiver. We treat it here as a constant because we are operating at such low frequencies. Second, the constant K2 that was calculated previously represents a measurement that was made on a particular day. In general, K2 is a function of, among many other parameters, the signal and local oscillator photodetector currents that the receiver was operating at on the day of the particular measurement. Since the phase noise spectrum measurements were taken on a different day, we had to renormalize the value of K2 by the ratio of the currents that were present on the day of the measurement as given in the above equation. Thirdly, V_π (the voltage that is required to shift the phase of the incoming light into the phase modulator by π degrees) is given above as 8 Volts. This value was not explicitly measured but was rather taken from the spec sheet of the phase modulator used. Knowing all of the above information, we can now compute the magnitude of A(f) under a simpler approximation as:

$$|A(f)| = \frac{\sqrt{((2\pi f\tau)^2\tau)^2 + (2\pi f)^2}}{\sqrt{\left[K1(1.1K2 + K3) - (2\pi f)^2\tau\right]^2 + \left[2\pi f(1 + 1.1K1K2\tau)\right]^2}} \tag{27}$$

Using this A(f), we can now generate a theoretical curve for the phase noise spectrum we should observe under lock. The relevant spectra are presented on the following pages in Figs. 16 and 17.

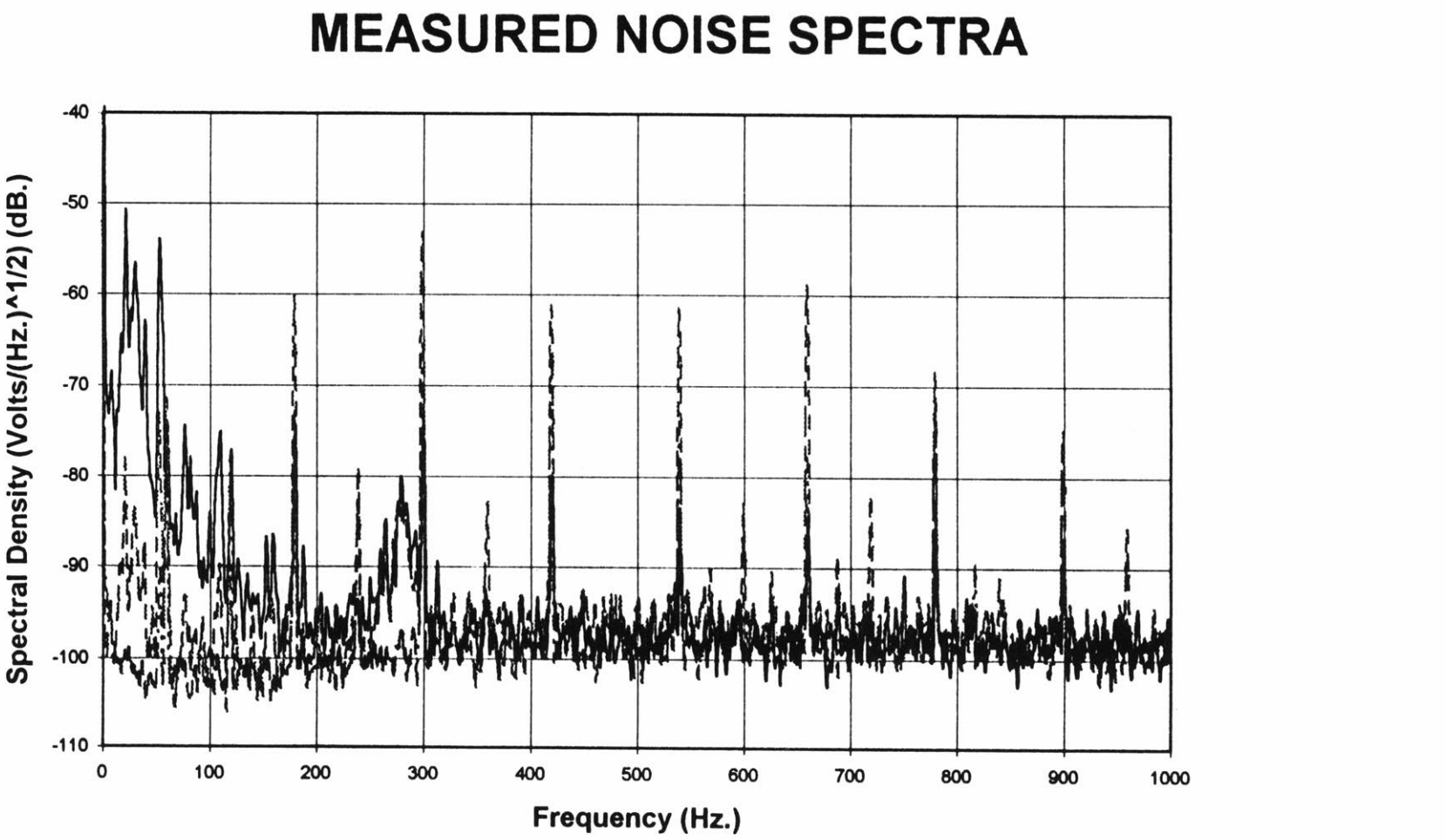

Fig. 16. Measured noise spectra showing the loop unlocked, locked, and the base level of electronic noise present.

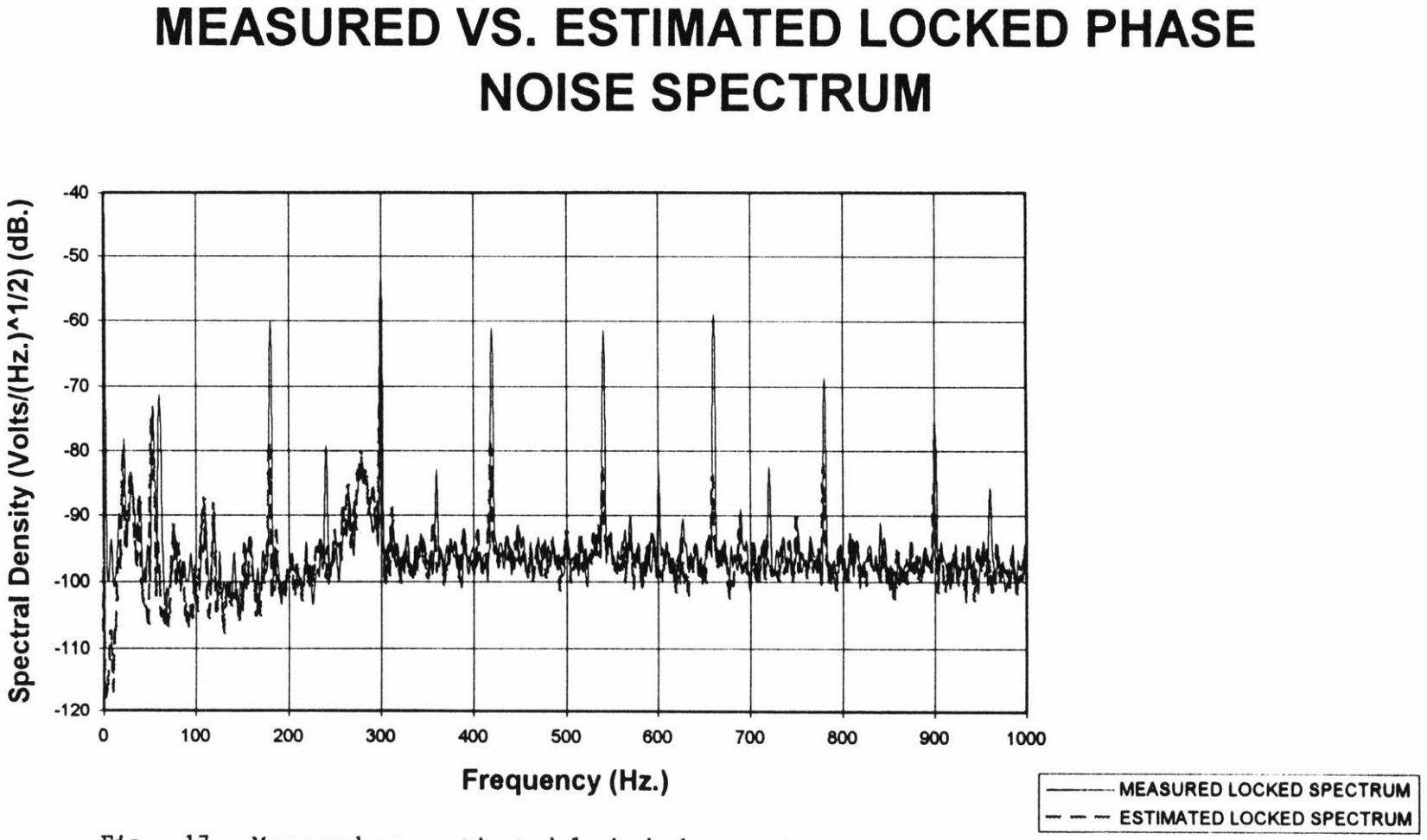

Fig. 17. Measured vs. estimated locked phase noise spectra.

In Fig. 16, we observe three measured noise spectra that are relevant to receiver's performance analysis. The electronic noise spectrum is roughly flat at about -100 dB. We can see the action of the phase-locked loop that was constructed in its suppression of the laser phase noise when it is locked. We can also observe that at higher frequencies, the dominant source of noise is the electronic noise. Finally, the spikes that can be observed are spaced 60 Hz. apart. These spikes do not represent receiver noise and were observed because the probe with which the measurement was made was picking up 60 cycle noise present in the room.

Fig. 17 shows two plots, the measurement of the power spectral density of noise in the phase-locked loop when it is locked and an estimate of this curve generated by the theoretical calculation presented above. Here, we can see good agreement between the measured and predicted curves. This fact is encouraging because we can be confident in analyzing the different types of noises in the system and how they affect the performance of the receiver.

Now it was necessary to calculate the total noise in the loop. We could do so by writing the expression for the variance deviation of the phase error in the phase lock loop:

$$\sigma_{TOT}^2 = \int_{-\infty}^{\infty} S_{\Phi,PN}(f)|1 - H(f)|^2 df + \int_{-\infty}^{\infty} S_{\Phi,SN}(f)|H(f)|^2 df + \int_{-\infty}^{\infty} S_{\Phi,EN}(f)|H(f)|^2 df \tag{28}$$

Here, H(f) represents the transfer function of the phase lock loop as it is typically presented in the literature on phase lock loop analysis [7]. It is calculated according to the topology in Fig. 15 as follows:

$$H(s) = \frac{\Phi_{c1}(s) + \Phi_{c2}(s)}{\Phi_{IN}(s)} = \frac{\Phi_{OUT}(s)}{\Phi_{IN}(s)} \tag{29}$$

Where $\Phi(s)$ is the Laplace transform of the phase waveform $\Phi(t)$ at the appropriate points in Fig. 15.

$$H(s) = \frac{K1K2\left(s + \frac{K2' + K3}{K2'\tau}\right)}{s^2 + s\left(K1K2 + \frac{1}{\tau}\right) + \frac{K1(K2' + K3)}{\tau}} \tag{30}$$

The transfer function in terms of frequency is given by:

$$H(f) = \frac{\alpha(j2\pi f + \beta)}{(j2\pi f)^2 + j2\pi f\gamma + \Delta} \tag{31}$$

$$\alpha = K1K2' \tag{32}$$

$$\beta = \frac{K2' + K3}{K2'\tau} \tag{33}$$

$$\gamma = K1K2' + \frac{1}{\tau} \tag{34}$$

$$\Delta = \frac{K1(K2' + K3)}{\tau} \tag{35}$$

Now we can proceed to evaluate the integrals above. Doing so, we obtain the following values for the various contributions to the total phase noise variance.

$$\sigma_{PN}^2 = 7.7 \times 10^{-6} rad^2$$
$$\sigma_{EN}^2 = 6.1 \times 10^{-5} rad^2$$
$$\sigma_{SN}^2 = 2.9 \times 10^{-16} rad^2$$
$$\sigma_{TOT}^2 = (.47^0)^2$$

We observe that the level of shot noise in our case is orders of magnitude smaller than the phase noise and the electronic noise. Furthermore, we can see that the electronic noise is the dominant source of noise. However, we also see that the total standard deviation of phase noise in the loop is less than 1 degree. Thus, theoretically, the number of data errors this receiver should have due to phase noise should be insignificant. However, as

we will show in 4.4, this receiver does not exhibit this kind of performance as demonstrated in the probability of error curve that was taken.

4.4 Probability of Error Test

A probability of error curve was measured for this receiver. It was found that the receiver operated at approximately 28 dB above the quantum limit of 9 photons per bit at a probability of error of 10^{-9}. This non-ideal performance must be explained. Since the standard deviation of phase error was less than 1 degree, it could not be the major cause of the discrepancy between the receiver's performance and the performance of an ideal system. A different explanation must be sought. The primary explanation is that the receiver had such a high level of front-end electronic noise power that it required a certain level of optical signal power to overcome that noise in order to operate at reasonable signal to noise ratios (i.e., there was a big optical power penalty due to the dominant electronic noise). To quantify this statement, it was necessary to calculate this power penalty and generate a theoretical probability of error vs. signal to noise ratio curve with this penalty built in. The power penalty should be a ratio of the electronic noise power to the shot noise power in the receiver. It was important to calculate these noise powers at the same place in the circuit. Since the level of electronic noise was measured at point A as represented in Fig. 11, we calculated this penalty there. Mathematically, we can write an expression for the theoretical power penalty.

$$PowerPenalty = \frac{S_{EN}B_{EN}}{4e\langle i_{LO,DC}\rangle B_{EN}\Gamma^2(50\Omega)^2} = 29dB \tag{36}$$

where we have,

$$S_{EN} = 4.5\times10^{-11}\left[\frac{V^2}{Hz.}\right]$$

$$B_{EN} = 950MHz.$$

$$\Gamma = \frac{G_R}{K_{PD}} = 867$$

$$K_{PD} = 7.1 \times 10^{-4} \left[\frac{V}{rad} \right]$$

$$i_{LO,DC} = .05 \times 10^{-3} A$$

Here Γ represents the gain factor from the point of the balanced front end to point A in Fig. 11. To obtain this value, we measured the gain of the phase detector represented by K_{PD}. S_{EN} is the value of the measured electronic noise floor as shown in Fig. 16 and represents a bilateral spectrum. B_{EN} is an estimate of the bandwidth over which that noise acts. We use 950 MHz. because that is the lowest frequency pole in the receiver (the cutoff frequency of the electronic filter preceding the decision and clock recovery chip). The theoretical value of 29 dB calculated in (36) is in fairly good agreement with the actual power penalty that was faced in the receiver. Any discrepancy between this value and the actual value is probably due to errors in the measured values such as the local oscillator photocurrent and the gain of the phase detector.

Now that we have accounted for the power penalty that was faced, it is necessary to calculate a theoretical probability of error curve for this receiver taking into account this penalty. To do this calculation, we proceeded in the following fashion. We measured several probability of error points and recorded the optical signal power at these points. Knowing this quantity and the level of electronic noise present in the receiver, we could compute a signal-to-noise ratio at each of these points. Then, we could plot these probability of error points vs. their respective signal to noise ratios and compare this curve to the probability of error curve for an ideal, shot-noise limited system. The signal-to-noise ratio is given by:

$$\left(\frac{S}{N}\right)_{meas} = \frac{\langle v_s(t) \rangle_A^{\,2}}{\langle v_n(t)^2 \rangle_A} = \frac{\left\langle 4\Gamma R \cos(\Delta\Phi(t) + p(t)\pi) \sqrt{P_{s,meas} P_{LO,meas}} \sqrt{1-k_s}\, 50\Omega \right\rangle^2}{S_{EN} B_{EN}} \qquad (37)$$

where we have,

$$R = .93\left[\frac{A}{W}\right]$$

$$P_{LO} = 5.2 \times 10^{-5} W$$

$$k_s = \frac{1}{8}$$

Here, R is the responsivity of the photodetectors and was calculated based on an estimate of the quantum efficiency of the photodetectors given in the spec sheet. K_S represents the amount of incoming optical power devoted to tracking.

Now we can plot the probability of error vs, the measured signal-to-noise ratio. Such a plot is shown on the next page in Fig. 18.

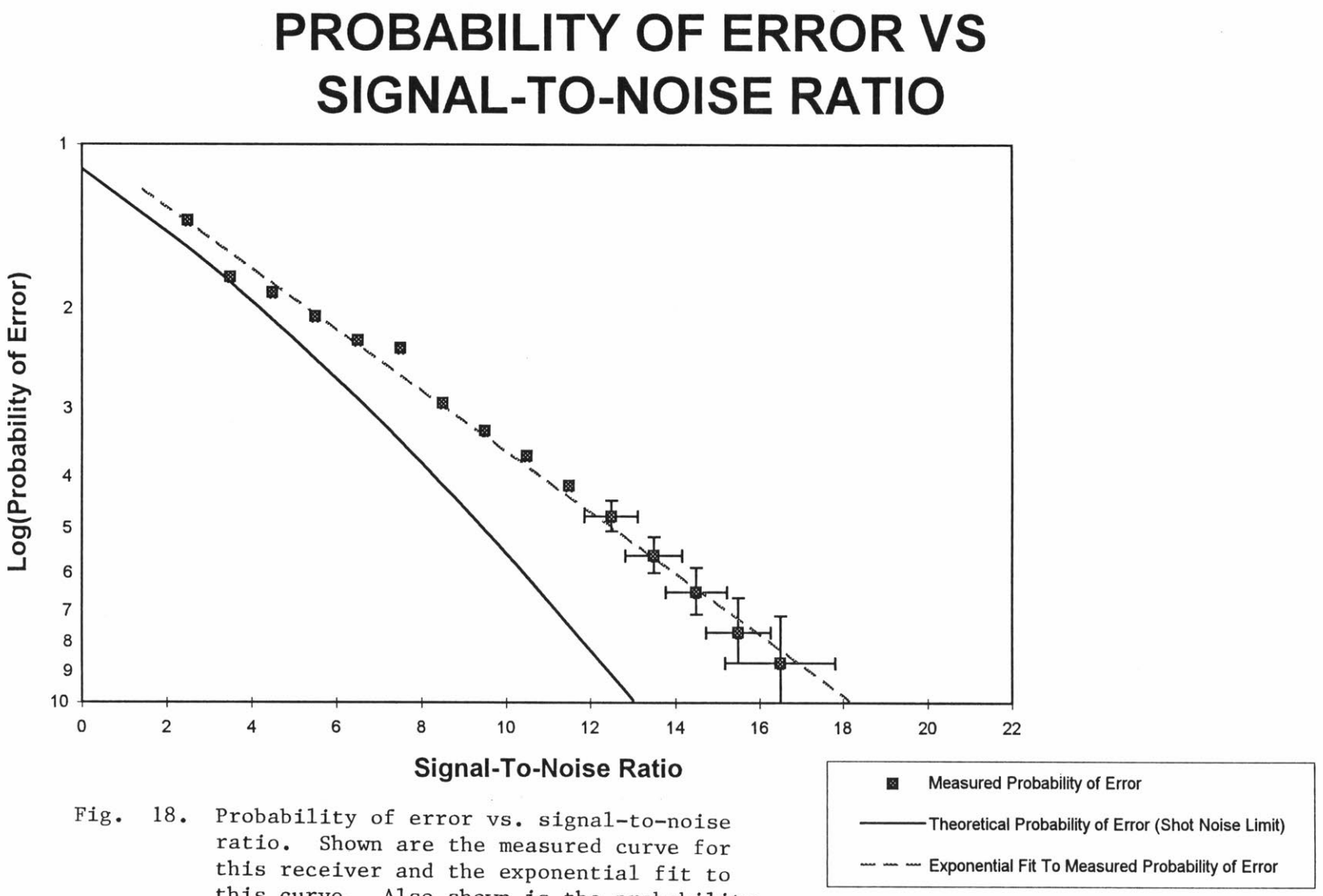

Fig. 18. Probability of error vs. signal-to-noise ratio. Shown are the measured curve for this receiver and the exponential fit to this curve. Also shown is the probability of error curve for an ideal, shot-noise limited receiver.

In Fig. 18, we see a discrepancy between the measured and calculated bit error rate curves. The discrepancy is not only in the horizontal position of the measured probability of error curve but also in its slope. The discrepancies are most likely due to more than one factor since the probability of error curve is a function of many interrelated factors. Some causes of the discrepancies might be due to one or all of the following: The measurements that were made have some error in them and therefore are not completely accurate. The vertical error bars in Fig. 18 represent the uncertainty of the probability of error measurement that was taken. These errors exit because there was uncertainty in the value read off of the probability of error tester. Uncertainty is also present in the measured signal-to-noise ratios because some of the quantities in (37), such as R, were estimated, rather than measured. In addition, some of the parameters in (37) were measured and there was a level of uncertainty in the measurements. The uncertainty in the signal-to-noise ratios is represented by the horizontal bars. Error bars are only shown on several points in the figure because at lower probabilities of error, the uncertainty in the measurement was too small to appear on the scale used. Finally, we must also consider the fact that the model we used to calculate a theoretical probability of error curve might not exactly describe the receiver that was built. As mentioned before, strong analogies can be made between the sync bit receiver and the typical decision-directed loop that was constructed by Wandernoth. However, the sync bit receiver has subtle differences in operation (i.e. the method by which the phase information is encoded, etc.) and these differences might cause the receiver to perform in a slightly different way than the model predicts. Furthermore, we must note that this experiment only used one laser source as both the signal laser and the local oscillator. This is a deviation from the original design of the receiver and was not modeled appropriately into the sync bit design. These and other factors are possible causes for the discrepancies between the actual and theoretical probability of error curves that were presented above. However, the disagreement in signal-to-noise ratios between the theoretical and measured curves in Fig. 18 is not drastic and is several dB in the worst case.

4.5 Thesis Table Setup and Scope Outputs

The next few pages show some key results that were obtained during the course of this experiment. Where necessary, an explanation of the picture is presented. Otherwise, the captions are self explanatory.

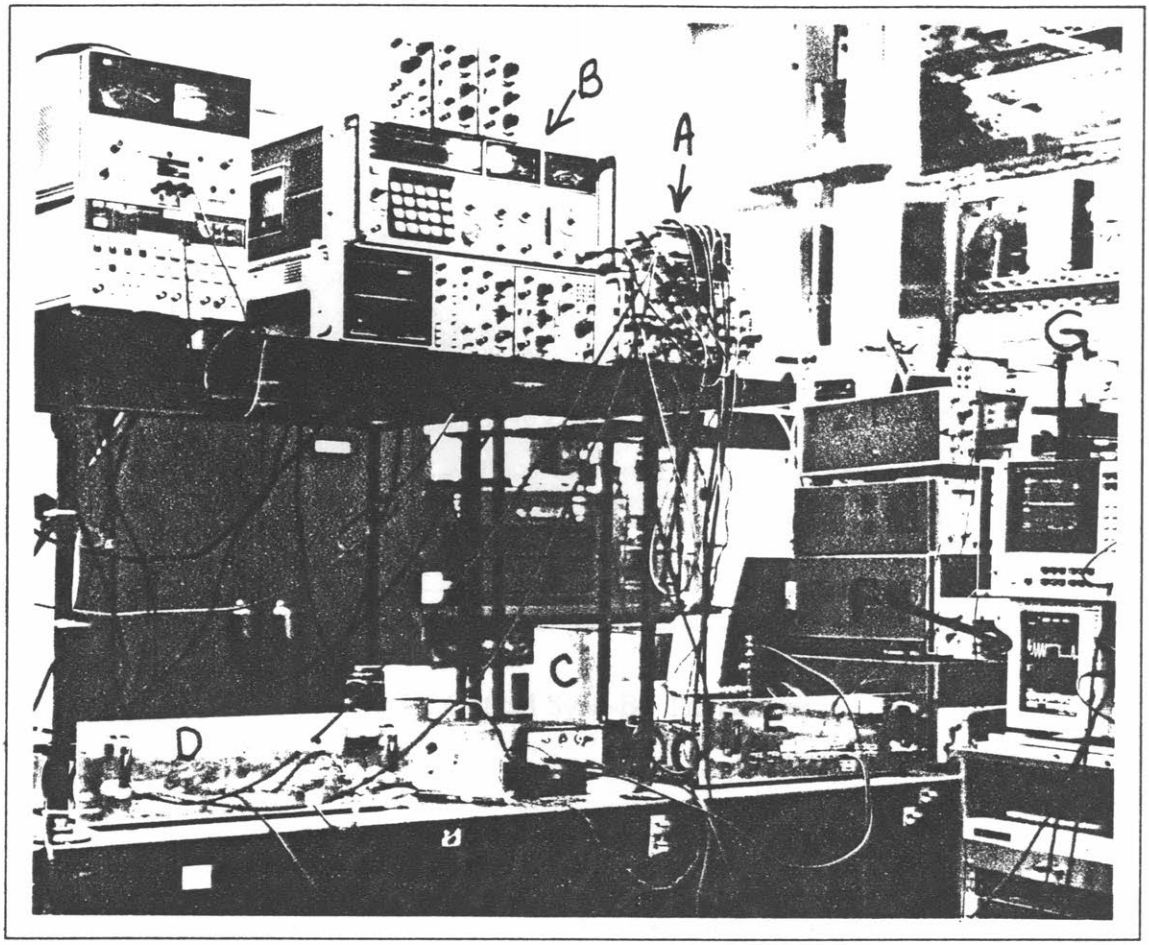

The table setup of the BPSK Optical Homodyne Receiver communications experiment can be seen here. The various pieces are represented by letters. **A** is the data source that was used to generate the 1.25 Gbit/s pseudorandom sequence. **B** is the 1.25 Ghz. clock source for the data generator. **C** is the box that contains the laser and all of the optical components of the interferometer. **D** is the sync bit transmitter that was built and **E** is the sync bit receiver. **F** is a digital sampling scope used to do most of the troubleshooting and data display. Finally, **G** is a dynamic signal analyzer that was used to perform loop transfer function and noise measurements.

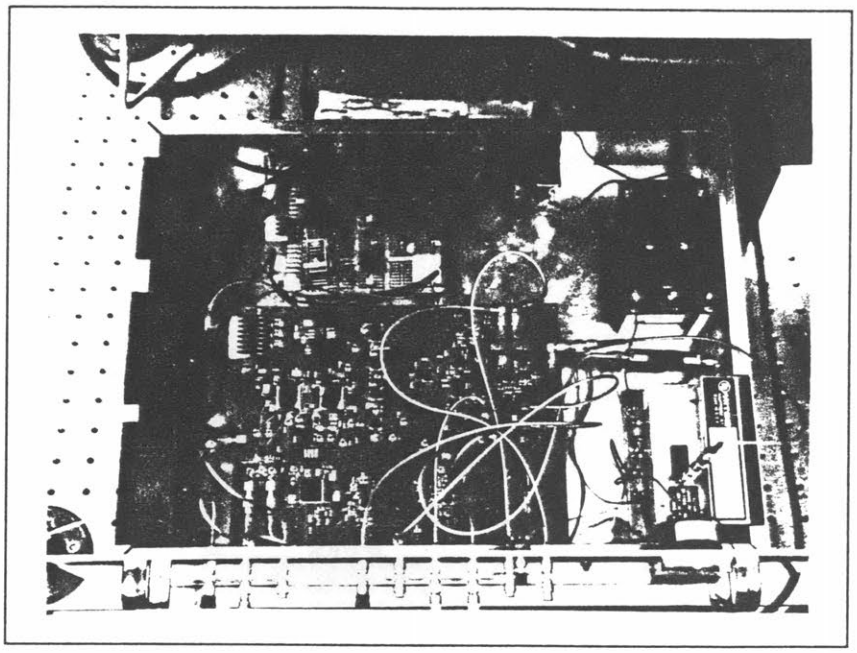

BPSK Optical Sync-Bit Transmitter

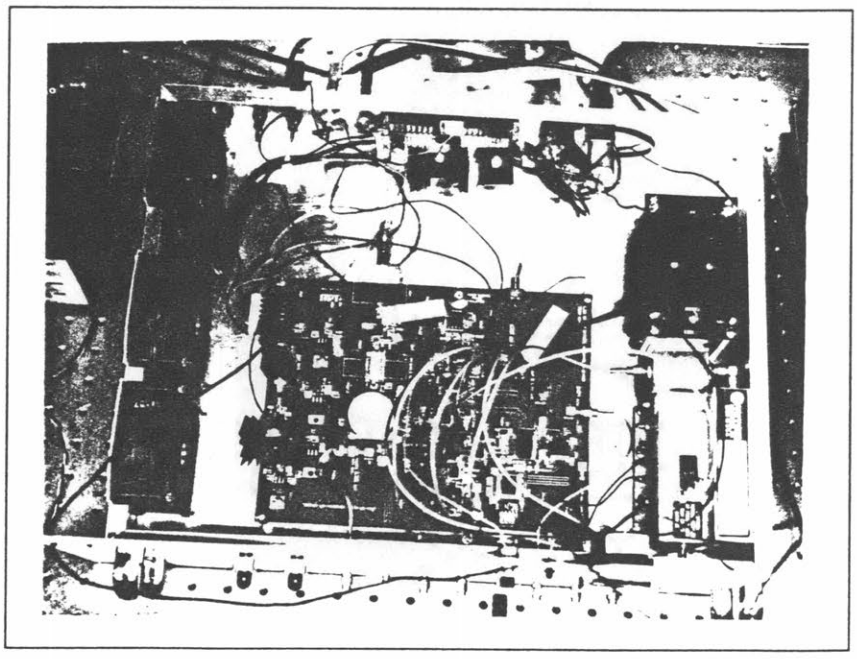

BPSK Optical Sync-Bit Receiver

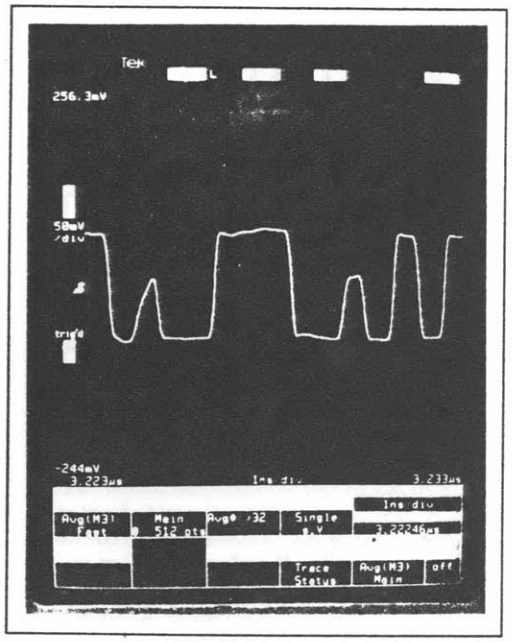

. Transmitter Output of the 1.429 Gbit/s Tri-Level Digital Waveform (Data + Sync Bits)

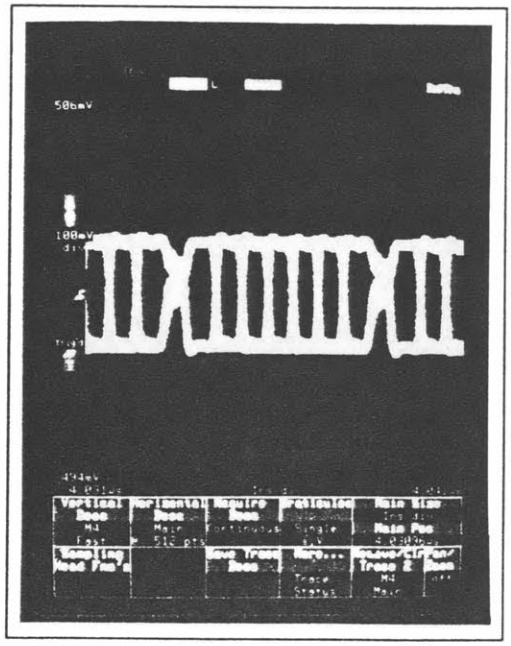

Transmitter Output of the 1.429 Gbit/s Data Eye (Data + Sync Bits)

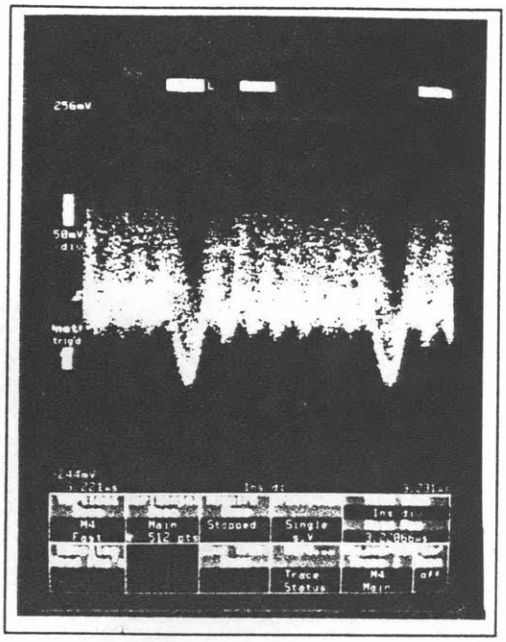

Detected 1.429 Gbit/s Data Eye (Loop Unlocked)

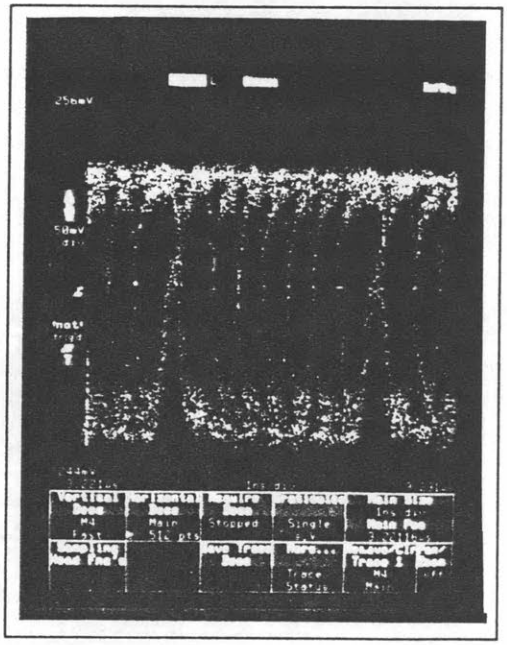

Detected 1.429 Gbit/s Data Eye (Loop Locked)

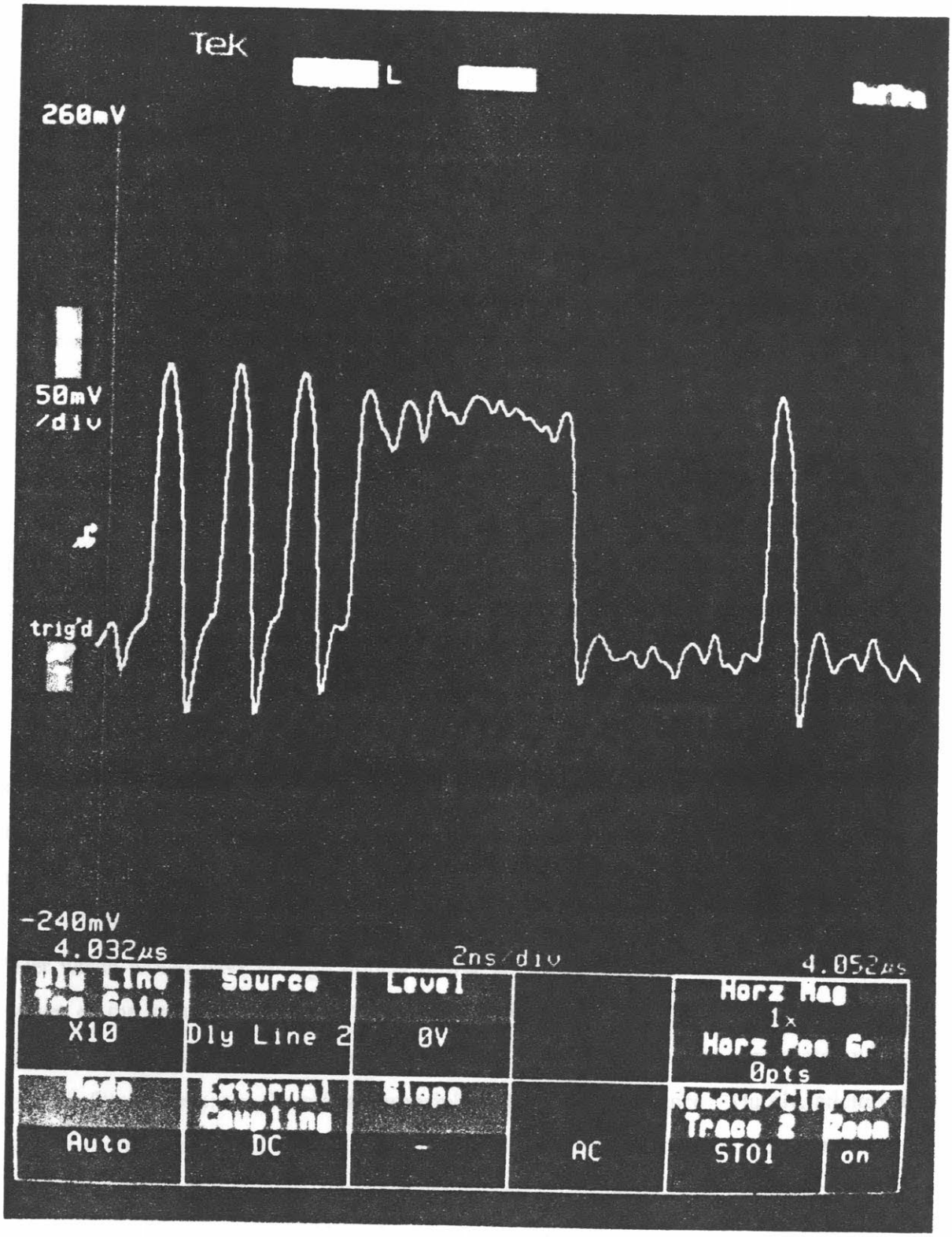

Receiver Output of 1.25 Gbit/s 2^7-1 Pseudorandom Sequence

CHAPTER 5

CONCLUSION

5.1 Conclusion

A homodyne receiver using synchronization bits has been constructed. A transmitter to produce the "sync bit" data waveform was also constructed. The receiver employed a decision-directed-like loop. The loop was observed to be locked for as much as 30 minutes at a time. Loop transfer function measurements were made and key parameters of the loop were extracted. The standard deviation of phase noise was modeled and was calculated based on loop measurements. The standard deviation of phase error was found to be 0.47 degrees. Furthermore, a theoretical probability of error curve was produced for the receiver. The receiver operated at 28 dB above the quantum limit for an ideal shot-noise limited PSK homodyne system at a BER of 10^{-9}. The receiver's measured probability of error curve was compared to a theoretical one that was calculated. It was found that the curves had only slight discrepancies between their slopes and their relative signal to noise ratios. These discrepancies could be partially explained by the uncertainty that existed in the measured and calculated quantities used to generate the probability of error curve for the receiver.

Significant improvements could be made to this receiver. First, we could obtain a laser which would have enough optical power so we could increase the level of optical power of the local oscillator laser to overcome the thermal and electronic noises in the receiver. In addition, an ideal second order phase-locked loop could be constructed with a lead lag filter to improve the overall probability of error performance. Thirdly, additional control could be provided to track the phase difference between two independent sources of light to make a "true" communications experiment rather than having one source acting as both the signal and local oscillator lasers.

BIBLIOGRAPHY

[1] J. R. Barry, "Performance of Coherent Optical Receivers," Electronics Research Laboratory Memorandum No. UCB/ERL M88/16, March 1988.

[2] A. Blanchard, *Phase-Locked Loops Application to Coherent Receiver Design.* Malabar, Florida: Krieger Publishing Company, 1992.

[3] M. Bopp, G. Huther, TH. Spatscheck, H. Specker, and Th. Wiesmann, "BPSK Homodyne and DPSK Heterodyne Receivers for Free-Space Communication with Nd:Host Lasers," *SPIE*, vol. 1522, pp. 199-209, 1991.

[4] A. W. Davis, M. J. Pettitt, J. P. King, and S. Wright, "Phase Diversity Techniques for Coherent Optical Receivers," *Journal of Lightwave Technology*, vol. LT-5, no. 4, pp. 561-572, 1987.

[5] G. Fischer, "A 700 Mbit/s PSK Optical Homodyne System with Balanced Phase Locked Loop," *Journal of Optical Communications*, vol. 9, pp. 27-28, 1988.

[6] J. Franz, "Evaluation of the Probability Density Function and Bit Error Rate in Coherent Optical Transmission Systems Including Laser Phase Noise and Additive Gaussian Noise," *J. Opt. Commun.*, vol. 6, pp. 51-57, 1985.

[7] F. M. Gardner, *Phaselock Techniques.* New York: John Wiley & Sons, 1979.

[8] R. Garreis and C. Zeiss, "90^0 Optical Hybrid for Coherent Receivers," *Optical Space Communications II*, SPIE, vol. 1522, pp. 210-219, 1991.

[9] J.G. Graeme, G. E. Tobey, and L.P. Huelsman, *Operational Amplifiers Design and Applications.* New York: McGraw-Hill Book Company, 1971.

[10] J. F. Hayes and W. C. Lindsey, "Power Allocation--Rapidly Varying Phase Error," *IEEE Transactions on Communications*, pp. 323-326, April, 1969.

[11] L. G. Kazovsky, "Balanced Phase-Locked Loops for Optical Homodyne Receivers: Performance Analysis, Design Considerations, and Laser Linewidth Requirements," *J. Lightwave Technology*, vol. LT-4, no. 2, pp. 182-195, 1986.

[12] L. G. Kazovsky, "Decision-Driven Phase-Locked Loops for Optical Homodyne Receivers: Performance Analysis, Design Considerations, and Laser Linewidth Requirements," *J. Lightwave Technology*, vol. LT-3, no. 6, pp. 1238-1247, 1985.

[13] W. R. Leeb, "Realization of 90^0 and 180^0 Hybrids for Optical Frequencies," *Report from the Institut fur Nachrichtentechnik, Technische Universitat Wien*, AEU, pp. 203-206, 1983.

[14] O. Lidoyne, P. Gallion, and D. Erasme, "Analysis of a Homodyne Receiver Using an Injection-Locked Semiconductor Laser," *Journal of Lightwave Technology*, vol. 9, no. 5, pp. 659-665, 1991.

[15] S. Norimatsu and K. Iwashita, "PLL Propagation Delay-Time Influence on Linewidth Requirements of Optical PSK Homodyne Detection," *J. Lightwave Technology*, vol. 9, no. 10, pp. 1367-1375, 1991.

[16] S. Norimatsu and K. Iwashita, "Linewidth Requirements for Optical Synchronous Detection Systems with Nonnegligible Loop Delay Time," *J. Lightwave Technology*, vol. 10, no. 3, pp. 341-348, 1992.

[17] S. Norimatsu, K. Iwashita, and K. Sato, "PSK Optical Homodyne Detection Using External Cavity Laser Diodes in Costas Loop," *IEEE Photonics Technology Letters*, vol. 2, no. 5, pp. 374-376, 1990.

[18] T. Okoshi and K. Kikuchi, *Coherent Optical Fiber Communications*. Boston, M.A.: Kluwer Academic Publishers, 1988.

[19] A. Papoulis, *Probability, Random Variables, and Stochastic Processes*. New York: McGraw-Hill Publishing Company, 1984.

[20] V. K. Prabhu, "PSK Performance With Imperfect Carrier Phase Recovery," *IEEE Transactions on Aerospace and Electronic Systems*, vol. AES-12, no. 2, pp. 275-285, 1976.

[21] S. A. Rhodes, "Effect of Noisy Phas Reference on Coherent Detection of Offset-QPSK Signals," *IEEE Transactions on Communications*, vol. com-22, NO. 8, pp. 1046-1055, 1974.

[22] J. Roberge, *Operational Amplifiers: Theory and Practice*. New York: John Wiley & Sons, 1975.

[23] F. G. Stremler, *Introduction to Communication Systems*. Reading, M.A.: Addison-Wesley Publishing Company, 1982.

[24] L. Sun and P. Ye, "Optical Homodyne Receiver Based on an Improved Balance Phase-Locked Loop with the Data-to-Phaselock Crosstalk Suppression," *IEEE Photonics Technology Letters*, vol. 2, no. 9, pp. 678-679, 1990.

[25] H. Tsao, Y. Lee, and J. Wu, "The Performance Analysis of Decision-Driven Optical Phase Locked Loop with Loop Delay," *J. Opt. Commun*, vol. 2, pp. 70-75, 1990.

[26] B. Wandernoth, "1064 nm, 565 Mbit/s PSK Transmission Experiment with Homodyne Receiver Using Synchronization Bits," *Electronics Letters*, vol. 27, no. 19, pp. 1692-1693, 1991.

Appendix A

Schematic and Layout Diagrams

This appendix includes schematic and layout diagrams of both the sync-bit transmitter and the sync-bit receiver. It is organized as follows. Page 77 shows the schematic diagram of the transmitter. Page 78 shows the layout diagram of the transmitter. Page 79 shows the schematic diagram of the receiver. Finally, page 80 shows the layout diagram of the receiver.

1.25 GBIT/S BPSK OPTICAL HOMODYNE TRANSMITTER

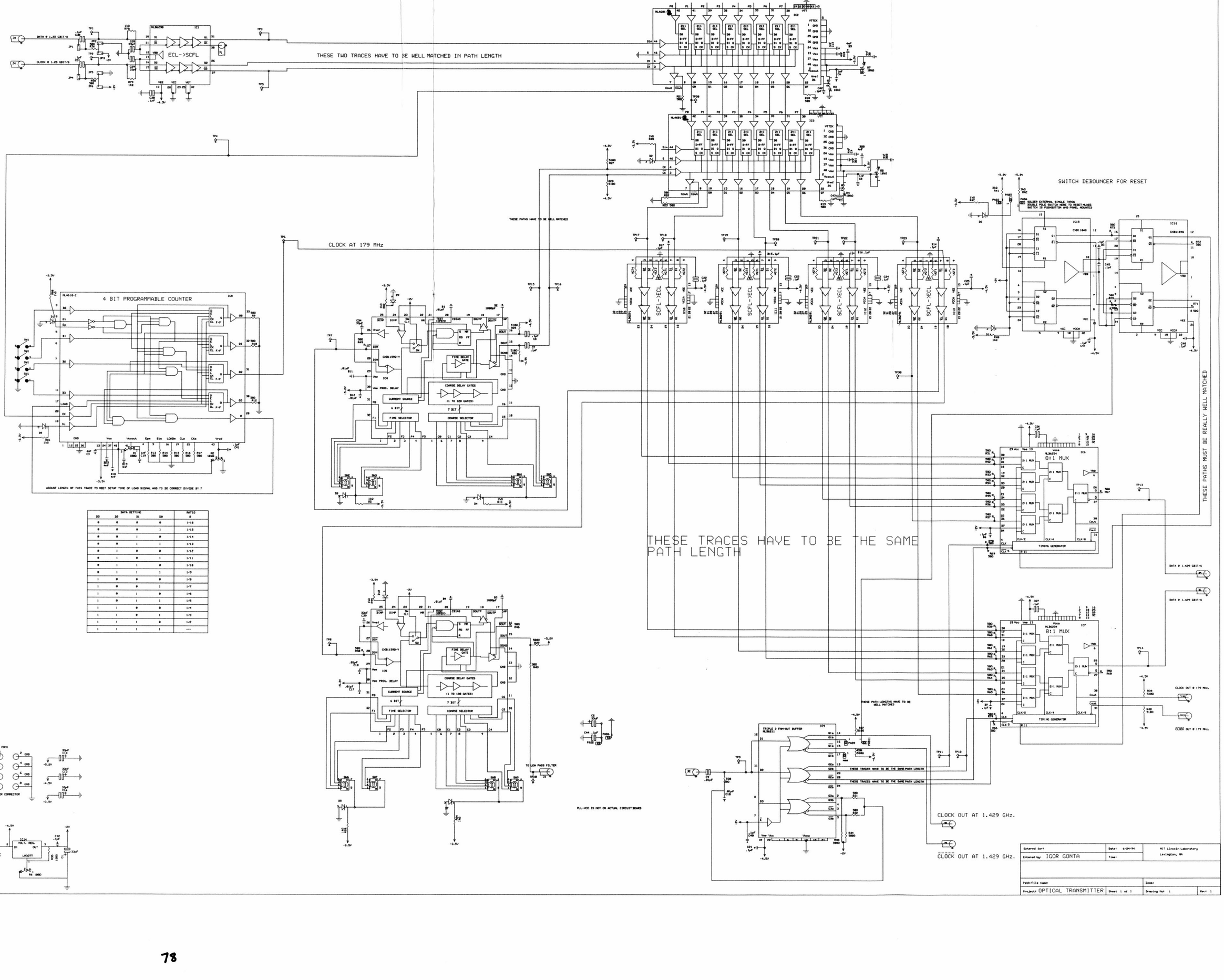

Data Setting				Ratio
D3	D2	D1	D0	R
0	0	0	0	1/16
0	0	0	1	1/15
0	0	1	0	1/14
0	0	1	1	1/13
0	1	0	0	1/12
0	1	0	1	1/11
0	1	1	0	1/10
0	1	1	1	1/9
1	0	0	0	1/8
1	0	0	1	1/7
1	0	1	0	1/6
1	0	1	1	1/5
1	1	0	0	1/4
1	1	0	1	1/3
1	1	1	0	1/2
1	1	1	1	---

THESE TRACES HAVE TO BE THE SAME PATH LENGTH

Entered Sort	Date: 6-26-96	MIT Lincoln Laboratory, Lexington, MA
Entered by: IGOR GONTA	Time:	
Path-File name:		Zoom:
Project: OPTICAL TRANSMITTER	Sheet 1 of 1	Drawing Mat 1 / Revt 1

.40 6.70 .20

.75

8.05

.50

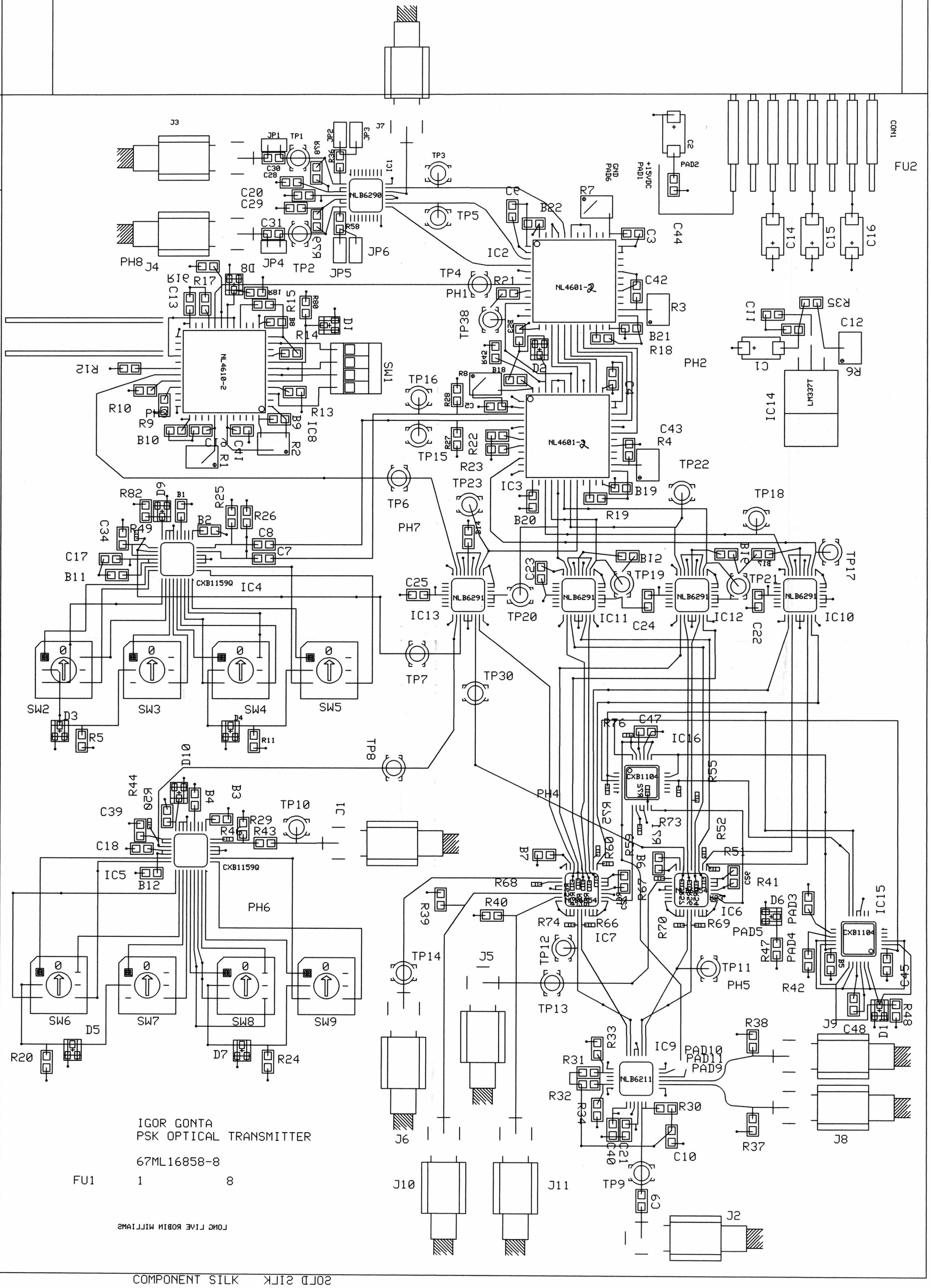

1.25 GBIT/S BPSK OPTICAL HOMODYNE RECEIVER

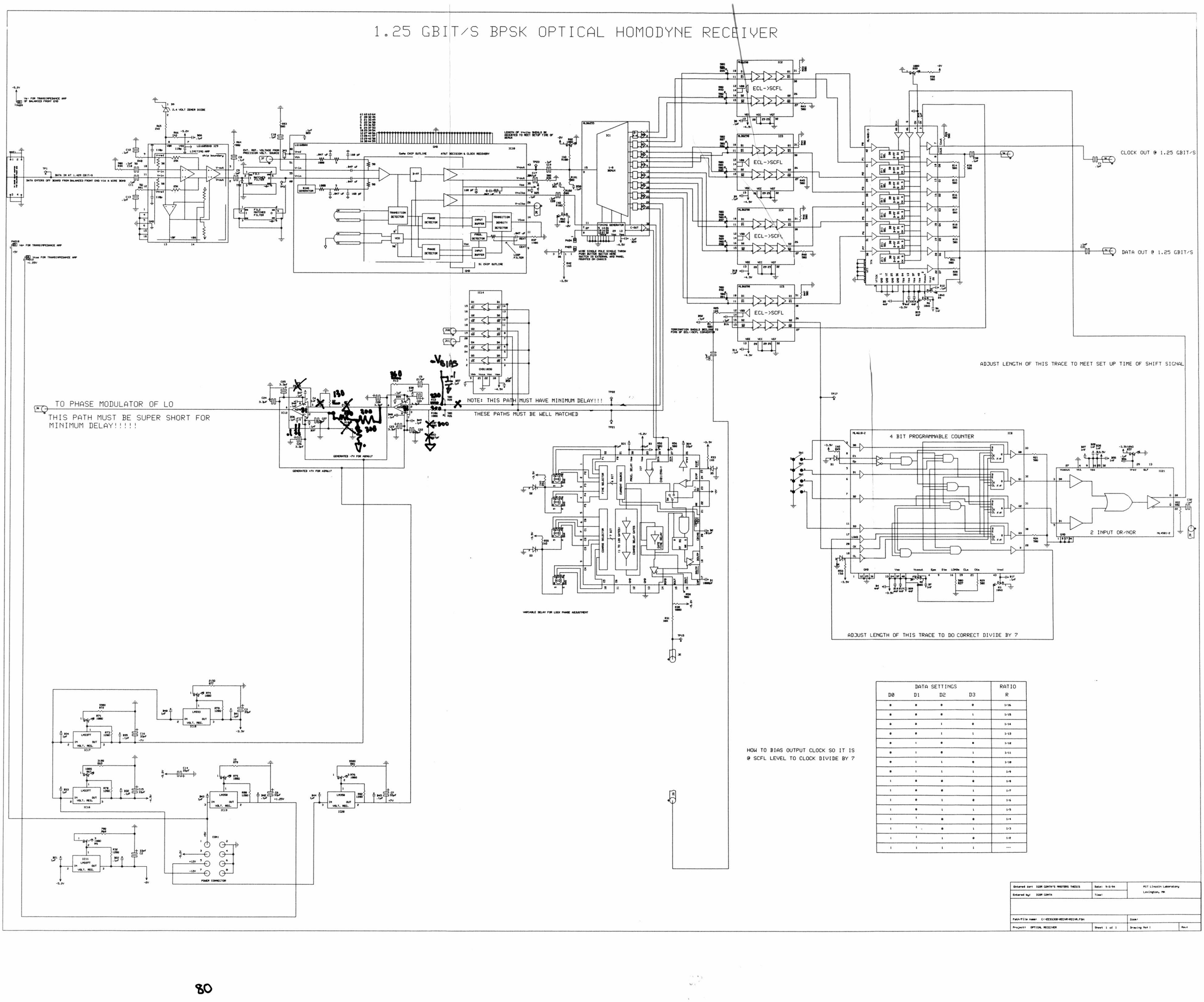

HOW TO BIAS OUTPUT CLOCK SO IT IS @ SCFL LEVEL TO CLOCK DIVIDE BY 7

DATA SETTINGS				RATIO
D0	D1	D2	D3	R
0	0	0	0	1/16
0	0	0	1	1/15
0	0	1	0	1/14
0	0	1	1	1/13
0	1	0	0	1/12
0	1	0	1	1/11
0	1	1	0	1/10
0	1	1	1	1/9
1	0	0	0	1/8
1	0	0	1	1/7
1	0	1	0	1/6
1	0	1	1	1/5
1	1	0	0	1/4
1	1	0	1	1/3
1	1	1	0	1/2
1	1	1	1	---

Entered on: IGOR GONTA'S MASTERS THESIS	Date: 9-2-94	MIT Lincoln Laboratory Lexington, MA
Entered by: IGOR GONTA	Time:	
Path-File name: C:\EE3308\RECVR-RECVR.PSH		Zoom:
Project: OPTICAL RECEIVER	Sheet 1 of 1	Drawing Not: Rev:

.20

6

.80

.500

1.25 GBIT/S OPTICAL HOMODYNE RECEIVER

IGOR GONTA

67ML16859-8

1 8

J1 | | DATA OUT @1.25 GBIT/S

SHIFT SIGNAL @ 179MHz.

J9 | C35 IC21

J5 | C1 IC6

CLOCK OUT @ 1.25 GHZ.

J4 | C30

CLOCK OUT @ 1.25 GHz.

FU2

PAD8

PAD9

PAD13

PAD1

PAD11

PAD12

PAD2

PAD7

PAD10

PAD6

ERROR SIGNAL TO PHASE MODULATOR

SYNC BIT

J10

J6 |

J11

SYNC BIT

EXT. THRESHOLD VOLT.

J7

J3

CLOCK @1.25 GHz.

J2 | |CLOCK @179 MHz.

MNT1

TP1

TP2

TP3

FIL1

FIL2

J8

RECOVERED CLOCK OUT
@ 1.429 GHz.

JP1 JP2 JP3

-5.2V
GND
+1.25V
GND
+5V
GND

+1.25V

-7V

+7V

4.5V

-3.5V

-2V

FU1

CON1

SW1 SW2 SW3 SW4

"Gather ye rosebuds while ye may"

COMPONENT SILK SOLDER SILK

8

.500